Available online at www.sciencedirect.com

ScienceDirect

Geochimica et Cosmochimica Acta 224 (2018) 96–115

Geochimica et Cosmochimica Acta

www.elsevier.com/locate/gca

The effects of metamorphism on iron mineralogy and the iron speciation redox proxy

Sarah P. Slotznick *, John M. Eiler, Woodward W. Fischer

Division of Geological and Planetary Sciences, California Institute of Technology, Pasadena, CA 91125, USA

Received 30 January 2017; accepted in revised form 4 December 2017; available online 10 December 2017

Abstract

As the most abundant transition metal in the Earth's crust, iron is a key player in the planetary redox budget. Observations of iron minerals in the sedimentary record have been used to describe atmospheric and aqueous redox environments over the evolution of our planet; the most common method applied is iron speciation, a geochemical sequential extraction method in which proportions of different iron minerals are compared to calibrations from modern sediments to determine water-column redox state. Less is known about how this proxy records information through post-depositional processes, including diagenesis and metamorphism. To get insight into this, we examined how the iron mineral groups/pools (silicates, oxides, sulfides, etc.) and paleoredox proxy interpretations can be affected by known metamorphic processes. Well-known metamorphic reactions occurring in sub-chlorite to kyanite rocks are able to move iron between different iron pools along a range of proxy vectors, potentially affecting paleoredox results. To quantify the effect strength of these reactions, we examined mineralogical and geochemical data from two classic localities where Silurian-Devonian shales, sandstones, and carbonates deposited in a marine sedimentary basin with oxygenated seawater (based on global and local biological constraints) have been regionally metamorphosed from lower-greenschist facies to granulite facies: Waits River and Gile Mountain Formations, Vermont, USA and the Waterville and Sangerville-Vassalboro Formations, Maine, USA. Plotting iron speciation ratios determined for samples from these localities revealed apparent paleoredox conditions of the depositional water column spanning the entire range from oxic to ferruginous (anoxic) to euxinic (anoxic and sulfidic). Pyrrhotite formation in samples highlighted problems within the proxy as iron pool assignment required assumptions about metamorphic reactions and pyrrhotite's identification depended on the extraction techniques utilized. The presence of diagenetic iron carbonates in many samples severely affected the proxy even at low grade, engendering an interpretation of ferruginous conditions in all lithologies, but particularly in carbonate-bearing rocks. Increasing metamorphic grades transformed iron in carbonates into iron in silicate minerals, which when combined with a slight increase in the amount of pyrrhotite, drove the proxy toward more oxic and more euxinic conditions. Broad-classes of metamorphic reactions (e.g. decarbonation, silicate formation) occurred at distinct temperatures-pressures in carbonates versus siliciclastics, and could be either abrupt between metamorphic facies or more gradual in nature. Notably, these analyses highlighted the importance of trace iron in phases like calcite, which otherwise might not be included in iron-focused research i.e. ore-system petrogenesis, metamorphic evolution, or normative calculations of mineral abundance. The observations show that iron is mobile and reactive during diagenesis and metamorphism, and these post-depositional processes can readily overprint primary redox information held by iron speciation. However, in principle, additional mineralogical and petrographic approaches can be combined with iron speciation data to help untangle many of these post-depositional processes and arrive at more accurate estimates of paleoenvironmental redox conditions and processes, even for metamorphosed samples.

* Corresponding author at: Earth & Planetary Science Department, University of California Berkeley, Berkeley, CA 94720, USA.
E-mail address: sslotz@berkeley.edu (S.P. Slotznick).

https://doi.org/10.1016/j.gca.2017.12.003
0016-7037/

1. INTRODUCTION

Iron is the most abundant transition metal in the crusts of rocky planets, planetary bodies, and asteroids (Lodders and Fegley, 1997), and it buffers (bio)geochemical redox processes. As a redox-sensitive element, the abundance of different iron-bearing phases within rocks can provide a window into the redox balance and oxygen levels/fugacity of the formation environment—whether it be deep in the mantle or on the surface within a sedimentary basin.

Early observations of changing iron abundance and mineralogy in sedimentary rocks documented the early Paleoproterozoic rise of atmospheric oxygen based on the transition from ferrous to ferric iron-bearing detrital minerals and paleosols leached of iron versus accumulation of ferric phases (Cloud, 1968; Holland, 1984; Roscoe, 1969; Rye and Holland, 1998). Since these seminal observations, a variety of geochemical techniques have been applied to understand ancient aqueous redox conditions based on diverse transition metal abundances and isotope ratios and even mineral species count (e.g. Hazen et al., 2008); among these proxies, one commonly applied is iron speciation.

Iron speciation is a bulk sequential chemical extraction technique to quantify the proportions of different iron phases in a given sample, which are interpreted using empirical calibrations of modern sedimentary environments to determine paleoredox state of the depositional environment: oxic, anoxic/ferruginous (<5 micromolar O_2), or euxinic (anoxic and sulfide bearing) (Poulton and Canfield, 2005; Raiswell and Canfield, 2012). Iron speciation data generated from a multitude of Precambrian successions suggest variable ferruginous, euxinic, and oxic waters between different intervals, basins, and facies within basins—cast upon what are thought to be dominantly ferruginous conditions (e.g. Poulton and Canfield, 2011; Sperling et al., 2015). This is distinctly different and far more complex than canonical views of the secular evolution of redox structure in sedimentary basins (ferruginous before ~2.3 Ga, then oxic surface waters with subsurface euxinia) (Canfield, 1998; Cloud, 1968). An additional complication for testing these alternative hypotheses is that other paleoenvironmental proxies (such as Mo isotopes) have used the redox interpretations from iron speciation as a basic assumption to develop methodology and build interpretive frameworks (e.g. Arnold et al., 2004; Kendall et al., 2009). Since iron speciation was calibrated for modern unlithified sediment, it is not well understood if processes associated with metamorphism, metasomatism, and diagenesis could alter the chemistry and mineralogy of samples in a way that could impact paleoenvironmental interpretations. This is important because all Precambrian sedimentary rocks have undergone some degree of post-depositional alteration. To evaluate and mitigate the potential impacts of metamorphism on "iron speciation space", we analyzed case examples of Phanerozoic sedimentary strata that have undergone a range of well-understood metamorphic transformations.

2. BACKGROUND

2.1. The iron speciation proxy

The iron speciation paleoredox proxy developed from work by Bob Berner and his students and colleagues at Yale to understand controls on the formation of pyrite in modern sedimentary environments (Raiswell and Canfield, 2012). In the method, iron is classified broadly into three hierarchical pools, each inclusive of the previous: pyrite iron (Fe_{py}), highly reactive (toward sulfide) iron (Fe_{HR}), and total iron (Fe_T). The ratio of Fe_{HR}/Fe_T is used to determine whether the depositional water column is oxic or anoxic, and then within anoxic waters, the ratio of Fe_{py}/Fe_{HR} is used to determine euxinic versus ferruginous water conditions (Fig. 1). As the proxy has evolved and been refined, different chemical extraction techniques have been used to resolve the various pools of iron (e.g. Table 1) adding a layer of complexity when applying or interpreting proxy data, which was calibrated and originally operationally-defined based on specific extraction steps.

The development of Fe_{py}/Fe_{HR} as an indicator for euxinic conditions is based on the Degree of Pyritization (DOP) ratio first developed by Soviet scientists using measurements of sulfur (e.g. Volkov, 1961) and then re-defined by Berner (1970) for iron analyses. The latter definition of DOP and Fe_{py}/Fe_{HR} are both metrics measuring how much of the reactive iron in a sample has been transformed to pyrite iron. The distinction between these proxies is that DOP defines Fe_{HR} as pyrite iron plus iron extracted using boiling HCl, but in recent years, alternative extraction methods for determining Fe_{HR} have become widely utilized (e.g. Leventhal and Taylor, 1990; Poulton and Canfield, 2005; Raiswell et al., 1994). DOP values were calibrated as euxinic if greater than 0.75 and oxic if less than 0.45 based on a survey of Cretaceous, Jurassic, and Devonian shales whose paleoredox conditions were independently determined from bioturbation and faunal assemblages (Raiswell et al., 1988). A later survey of modern siliciclastic sediments suggested instead that DOP values <0.4 indicated oxic environments, but many euxinic environments had

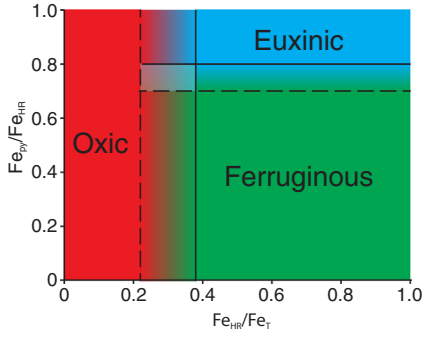

Fig. 1. Iron speciation cross-plot with ratio of pyrite iron to highly reactive iron (Fe_{py}/Fe_{HR}) plotted against highly reactive iron to total iron (Fe_{HR}/Fe_T) with paleowater column redox conditions bounded by limits from empirical calibrations discussed in text.

Table 1
Sequential extraction method utilized by most iron speciation studies and targeted minerals.

Pool	Short name[a]	Details	Extractable Fe from minerals[b]	Source[c]
Fe_{carb}	Acetate	(1) 1 M Na Acetate, pH 4.5, 24 h room temperature or 48 h 50 °C	Carbonate iron, siderite, ankerite (pyrrhotite)	1
Fe_{ox1}	Hydroxylamine	(2) 1 M Hydroxylamine-HCl, 48 h	Ferrihydrite, lepidocrocite	1
Fe_{ox2}	Dithionite	(3) Na dithionite solution (50 g l^{-1}), pH 4.8, 2 h	Goethite, akaganéite, hematite (ferrihydrite, lepidocrocite)	1
Fe_{mag}	Oxalate	(4) 0.2 M ammonium oxalate/0.17 M oxalic acid, pH 3.2, 6 h	Magnetite (titanomagnetite, ilmenite, goethite, ferrihydrite, lepidocrocite, siderite, pyrrhotite)	1,2,3,4
Fe_{PRS}	Boiling HCl	(5) 12 M HCl, 1 min boiling	Poorly reactive sheet silicates like nontronite, biotite, chlorite, glauconite (all of the above)	1,5
Fe_{py}	CRS	Chromium reduction with 1 M $CrCl_2$ solution, 2 h boiling + Zn, Ag distillation	Pyrite (pyrrhotite, S, Ni-Zn-Cu-As-Cd-Pb sulfides)	1,6,7
Fe_U	–	Total iron (from XRF, ashing and boiling in 6 M HCl, etc.) minus above sum	Silicates	1
–	AVS	Several options using HCl of different strengths, temperatures, times ± chlorides	Monosulfides like amorphous FeS, mackinawite, greigite, pyrrhotite	8,9

[a] Abbreviations: CRS = chromium-reducible sulfide, AVS = acid-volatile sulfide.
[b] Minerals in parenthesis are those that can be extracted in this step, but should already have been extracted using the sequential extraction technique or are not the targeted minerals.
[c] References: (1) Poulton and Canfield (2005), (2) Dold (2003), (3) Algoe et al. (2012), (4) Burton et al. (2006), (5) Raiswell et al. (1994), (6) Canfield et al. (1986), (7) Schumann et al. (2012), (8) Cornwell and Morse (1987), (9) Praharaj and Fortin (2004).

DOP < 0.75—the discordance was attributed to particularly high detrital fluxes, sample oxidation, and decreased diagenesis (Raiswell and Canfield, 1998). As studies moved toward using Fe_{HR} extractions in which highly reactive iron is extracted using dithionite instead of boiling HCl, calculations were performed for Fe_{py}/Fe_{HR} to show that Fe_{py}/Fe_{HR} values average 0.87 for euxinic deep Black Sea samples, 0.65 for Black Sea shelf sediments, and 0.61 for dysoxic marine samples (data from Anderson and Raiswell, 2004; Raiswell and Canfield, 1998). From this data, an upper limit of $Fe_{py}/Fe_{HR} = 0.8$ was chosen for ferruginous conditions (Poulton and Canfield, 2011; Raiswell and Canfield, 2012). Today, a distinct 5-step sequential extraction technique for Fe_{HR} is the standard methodology (Table 1) (Poulton and Canfield, 2005), but no further calibrations on large surveys of sediment or rocks have been performed for Fe_{py}/Fe_{HR}. However, a study on Cretaceous marine shale from Ocean Anoxic Event 3 independently confirmed euxinic depositional conditions based on lack of bioturbation and concentrations of sulfurized organic matter and chalcophilic trace elements as a test of the proxy; ratios of Fe_{py}/Fe_{HR} corroborated the upper limit of 0.8 and suggested a lower limit of euxinia at $Fe_{py}/Fe_{HR} = 0.7$ (März et al., 2008). These limits have become standard (Fig. 1), and have been widely applied to differentiate euxinic and ferruginous conditions of Precambrian-age rocks (Poulton and Canfield, 2011; Raiswell and Canfield, 2012; Sperling et al., 2015).

Although the anoxia proxy was developed independently, today most studies pair the Fe_{HR}/Fe_T anoxia proxy with the Fe_{py}/Fe_{HR} euxinia proxy discussed above (first done by Shen et al., 2002). A primary focus of the Raiswell and Canfield (1998) survey of modern siliciclastic sediments was to understand the abundances of highly-reactive iron (extracted using dithionite). They discovered that oxic and dysoxic sediments had $Fe_{HR}/Fe_T < 0.38$. Samples from modern euxinic and anoxic basins contained Fe_{HR}/Fe_T ratios primarily above 0.38, but included values down to 0.18. Phanerozoic shales deposited in normal oxic marine conditions, based on faunal assemblages and DOP values, had a Fe_{HR}/Fe_T average of 0.14, significantly lower than the modern sediment average of 0.26 (Poulton and Raiswell, 2002). Additionally, a detailed test of Fe_{HR}/Fe_T on the Jurassic Kimmeridge Clay highlighted that Fe_{HR}/Fe_T ratios tracked well with interpretations of oxygen limitation and anoxia determined by faunal assemblages and bioturbation (Raiswell et al., 2001). Based on these compilations and analysis, the paleoredox proxy was defined as having a lower Fe_{HR}/Fe_T limit of 0.22 for anoxic sediments and an upper limit of oxic conditions at 0.38 (Fig. 1) (Poulton and Canfield, 2011). It is worth noting that the Fe_{HR}/Fe_T limits were not updated for newer sequential extraction techniques (e.g. Poulton and Canfield, 2005); a test on modern carbonate samples from a range of oxic and anoxic environments using the new sequential extraction technique suggested that the Fe_{HR}/Fe_T limits were similar (Clarkson et al., 2014). However, a direct method comparison on Ordovician mudstones and siltstones suggested Fe_{HR}/Fe_T was significantly lower using the older extraction method of a single dithionite step (Farrell et al., 2013). The authors note that this discrepancy highlights a problematic skew toward anoxia for recent sequential extraction studies as redox interpretations of the data are made using the limits defined by the older dithionite extraction method.

2.2. Sequential extraction pools

Bulk sequential extraction techniques are helpful because they provide quantitative results; however, questions often exist as to whether the targeted phases are being accurately extracted or not. Today most studies presenting iron speciation data to infer paleoredox conditions follow the sequential extraction technique developed by

Poulton and Canfield (2005) with slight modifications depending on the samples, mineralogy, and specific lab group protocol. This technique keeps Fe_{py} the same and divides the Fe_T and Fe_{HR} pools as such:

$$Fe_{HR} = Fe_{carb} + Fe_{ox1} + Fe_{ox2} + Fe_{mag} + Fe_{py}$$

$$Fe_T = Fe_U + Fe_{PRS} + Fe_{HR}$$

where Fe_{carb} is the iron carbonate pool (acetate extraction), Fe_{ox1} is the "easily reducible" ferric iron oxide pool (hydroxylamine extraction), Fe_{ox2} is the ferric iron (hydr)oxide pool (dithionite extraction), Fe_{mag} is the magnetite pool (oxalate extraction), Fe_{PRS} is the poorly reactive sheet silicate pool (boiling HCl extraction), and Fe_U is the unreactive pool (based on subtraction) (see Table 1 for additional details). The addition of these extra extraction steps is to target magnetite and iron-rich carbonates (Poulton and Canfield, 2005; Raiswell and Canfield, 2012).

Even with these new targeted phases, there are still several iron-bearing (and sulfur-bearing) minerals present in ancient rocks that can be extracted during the iron speciation steps, but are not explicitly defined (e.g. Tables 1, 2). Notably, because of its variable chemistry, pyrrhotite is entirely or partially dissolved during the Fe_{carb} extraction (Poulton and Canfield, 2005; Reuschel et al., 2012), potentially with more extracted in the Fe_{ox} or Fe_{mag} extractions (e.g. Chang and Kirschvink, 1985), and can also be extracted in the Fe_{py} pool (Partin et al., 2015; Praharaj and Fortin, 2004; Schumann et al., 2012); therefore additional extraction steps and calculations are often included when pyrrhotite may be present. Pyrrhotite is typically grouped with the Fe_{py} pool with the assumption that it formed either as a primary phase or from pyrite, and in either case marks euxinic depositional conditions (e.g. Asael et al., 2013; März et al., 2008; Reuschel et al., 2012).

There is lingering debate about the accuracy of various sequential extraction techniques in diagenetically stabilized sedimentary rocks (Praharaj and Fortin, 2004; Raiswell et al., 2011; Reinhard et al., 2009; Reuschel et al., 2012) and even in modern sediments and soil (Bacon and Davidson, 2008; Egger et al., 2014; Hanahan, 2004; Hsieh et al., 2002; La Force and Fendorf, 2000). Our approach in this study is to assume the chemical extractions accurately extract the targeted phases and instead probe a set of questions about the iron speciation proxy arising from changes in chemistry and mineralogy that occur during metamorphism of sedimentary rocks.

2.3. Previous work on the effects of metamorphism on the iron speciation paleoredox proxy

As development of the iron speciation proxy continues and it is applied to older and more mineralogically complex samples, efforts have been made to understand how iron moved during diagenesis/metamorphism and to attempt to recreate the original iron pools (e.g. Asael et al., 2013; Partin et al., 2015; Raiswell et al., 2011; Reinhard et al., 2013). Testing for pyrrhotite is one such adjustment, although calculation of "original" iron can be difficult since pyrrhotite has variable stoichiometry and in both acid-volatile sulfide (AVS) and chromium-reducible sulfide (CRS) extractions, the sulfur is measured not the iron. Studies have sought to calculate pyrrhotite stoichiometrically (e.g. Asael et al., 2013; Cabral et al., 2013) while other times it is simply grouped with pyrite which under-estimates the amount of iron (e.g. Li et al., 2015; Partin et al., 2015). The question of authigenic syndepositional or diagenetic pore-water phases has been addressed by Raiswell et al. (2011) who provided an additional extraction method to more precisely measure iron carbonate phases and a new proxy for authigenic iron defined as iron extracted from poorly reactive silicates (such as mica and chlorite), carbonates, oxides, and pyrite. However, these developments do not address the timing of when these authigenic phases formed and whether they accurately capture water column redox conditions during deposition—analyses on paired Triassic limestone and dolomite samples show burial dolomitization increases Fe_{HR}/Fe_T ratios and some low-iron modern oxic carbonates also show enrichments in Fe_{HR}/Fe_T above the 0.38 oxic limit, interpreted to be from diagenetic dolomitization or pyrite formation (Clarkson et al., 2014).

The effect on iron speciation of iron movement between the silicate, highly reactive, and pyrite pools has also been examined using simple models. Movement of iron from carbonates and oxides to silicate phases will increase Fe_{py}/Fe_{HR} values and lower Fe_{HR}/Fe_T values making paleoredox appear more euxinic and more oxic; the latter ratio and paleoredox change will also occur with authigenic formation of iron silicates (Reinhard et al., 2013). The formation of pyrrhotite from pyrite by loss of sulfur from the system without any iron movement will tend to lower both Fe_{HR}/Fe_T and Fe_{py}/Fe_{HR} ratios in ferruginous systems making basins appear more oxic and more ferruginous respectively; if iron sulfides are the main highly-reactive mineral, possible in some euxinic environments, Fe_{py}/Fe_{HR} would be less affected (Reinhard et al., 2013). In this study, we expanded upon this previous work by considering additional reactions of iron-bearing phases, using data from metamorphosed sedimentary rocks as test-cases, and increasing the span of studied metamorphic conditions.

3. METHOD

We selected known reactions that occur during metamorphism and plotted their vectors in the iron speciation cross-plot aka "iron speciation space" to show possible effects on the paleoredox proxy that occur with increasing temperatures and pressures. With knowledge of mineralogical abundances and chemistry, we were able to convert information about a sample's mineralogy into iron abundance, iron speciation ratios, and paleoredox interpretations. Mineral abundance was given by mineralogical assemblages in petrographic studies and by stoichiometry in metamorphic reactions. The amount of iron in a mineral was determined based on its formula (as given by the reference or, if not given, as in Table 2) and then mineralogy was converted into iron abundance. Each mineral was partitioned into an iron pool following the current standard extraction techniques (Poulton and Canfield, 2005) (Table 1): pyrite, carbonate, ferric oxide, magnetite, poorly

Table 2
Key minerals identified within the Waits River, Gile Mountain, Waterville, and Sangerville-Vassalboro Formations.

Name	Abbr.[a]	General formula	Assumed formula	Assigned iron pool
Fe-bearing minerals				
Muscovite	ms	$KAl_2(AlSi_3O_{10})(OH)_2$	–	Fe_{PRS}
Paragonite	pg	$NaAl_2(AlSi_3O_{10})(OH)_2$	–	Fe_{PRS}
Biotite	bt	$K(Mg,Fe)_3(AlSi_3O_{10})(F,OH)_2$	–	Fe_{PRS}
Chlorite	chl	$(Al,Fe,Mg,Mn,Ti)_{5\text{-}6}(Al,Fe,Si)_4(O,OH)_{18}$	–	Fe_{PRS}
Calcite	cal	$CaCO_3$	–	Fe_{carb}
Ankerite	ank	$Ca(Fe,Mg,Mn)(CO_3)_2$	$CaFe_{0.5}Mg_{0.5}(CO_3)_2$[b]	Fe_{carb}
Ilmenite	ilm	$FeTiO_3$	$FeTiO_3$[c]	Fe_{mag}
Pyrrhotite	po	$Fe_{(1-x)}S$ (x = 0–0.2)	$Fe_{0.95}S$ or $Fe_{0.907}S$[d]	Fe_{carb} or Fe_{py}
Pyrite	py	FeS_2	FeS_2	Fe_{py}
Chalcopyrite	ccp	$CuFeS_2$	$CuFeS_2$	Fe_{py}
Epidote	ep	$Ca_2Al_2Fe(Si_2O_7)(SiO_4)O(OH)$	–	Fe_U
Allanite	aln	$(Ce,Ca,Y,La,etc.)_2(Al,Fe)_3(SiO_4)_3(OH)$	$CeCaFe_{1.5}Al_{1.5}(SiO_4)_3(OH)$	Fe_U
Clinozoisite-Zoisite	zo	$Ca_2Al_3(Si_2O_7)(SiO_4)O(OH)$	–	Fe_U
Garnet	grt	$(Ca,Mg,etc.)_3(Fe,Al,Ti,etc.)_2(SiO_4)_3$	–	Fe_U
Staurolite	st	$Fe_2Al_9Si_4O_{23}(OH)$	$Fe_2Al_9Si_4O_{23}(OH)$[e]	Fe_U
Diopside	di	$CaMgSi_2O_6$	–	Fe_U
Amphibole	amp	$(Na,K,Ca,Pb,[])(Li,Na,Mg,Fe,Mn,Ca)_2$ $(Li,Na,Mg,Fe,Mn,Zn,etc.)_5(Si,Al,Ti)_8O_{22}(OH,F,Cl,O)_2$[f]	–	Fe_U
Tourmaline	tur	$(Ca,Na,K,[])(Al,Fe,Li,Mg,Mn)_3$ $(Al,Cr,Fe,V)_6Si_6O_{18}$ $(BO_3)_3(O,OH)_3(F,O,OH)$[f]	$NaFeMg_2Al_6(Si_6O_{18})(BO_3)_3(OH)_3(OH)$	Fe_U
Non-Fe bearing minerals				
Quartz	qz	SiO_2	–	–
Plagioclase	pl	$NaAlSi_3O_8$ – $CaAl_2Si_2O_8$	–	–
Sphene	spn	$CaTi(SiO_4)O$	–	–
Rutile	rt	TiO_2	–	–
Graphite	gr	C	–	–
Alkali feldspar	afs	$KAlSi_3O_8$	–	–
Kyanite	ky	$Al_2(SiO_4)O$	–	–
Apatite	ap	$Ca_5(PO_4)_3(F,Cl,OH)$	–	–
Zircon	zrn	$Zr(SiO_4)$	–	–
Monazite	mnz	$(Ce,La,Nd,Th,Sm,Gd)PO_4$	–	–
Scapolite	scp	$Na_4Al_3Si_9O_{24}Cl$ – $Ca_4Al_6Si_6O_{24}CO_3$	–	–

[a] Abbreviations for minerals following Whitney and Evans (2010), used in Table 3.
[b] Assumed formula only used for trace amounts in Léger and Ferry (1991).
[c] Assumed formula is used in all studies except Gile Mountain and Waits River Formation data from Ferry (1994) and Ferry (2007).
[d] $Fe_{0.95}S$ was used as the assumed formula for the Waits River and Gile Mountain Formation samples. $Fe_{0.907}S$ was used as the assumed formula for the Waterville and Sangerville-Vassalboro Formation samples since this is the average pyrrhotite composition from 18 samples in the Waterville Formation (Ferry, 1981).
[e] Assumed formula only used for trace amounts in Ferry (1994).
[f] [] stands for no element in this structural position.

reactive sheet silicates, or unreactive silicates. The assignments used for all minerals are noted in Table 2. Ilmenite was included in Fe_{mag} due to sequential extraction methodology studies, although it may not actually be "highly reactive" toward sulfides. Pyrrhotite's assignment was complicated; as discussed above, if studies did not test for pyrrhotite then it would be extracted in Fe_{carb}, but today many studies have started to include a separate extraction test in which case pyrrhotite is grouped with Fe_{py}. In order to have our models comparable to both modern and older iron speciation studies, we performed two sets of calculations with pyrrhotite in either the Fe_{carb} or Fe_{py} pool. After the iron per pool was summed, non-dimensional ratios of Fe_{py}/Fe_{HR} and Fe_{HR}/Fe_T could be calculated; for metamorphic reactions, changes in these ratios from product to reactant allowed uniform-intensity reaction vectors to be plotted in iron speciation space.

4. IRON IN METAMORPHIC REACTIONS

Iron is mobile during metamorphism from subgreenschist facies rocks through high metamorphic grades. One of the most studied low-grade iron transitions is the transformation of pyrite into pyrrhotite due to its importance as a sulfur buffer during metamorphism. Pyrite is stable at low pressures up to 742 °C after which elemental iron, sulfur, and pyrrhotite dominate the Fe-S system (Vaughan and Craig, 1997). Except for the FeS endmember (troilite), pyrrhotite is "metastable" at room temperature since it is not thermodynamically stable yet appears in nature (Vaughan and Lennie, 1991); thermodynamic experiments and calculations indicate the formation of pyrrhotite from pyrite begins at ~75–200 °C (Hall, 1986; Kissin and Scott, 1982) and evolves following the commonly used pyrrhotite-pyrite buffer curve depending on temperature and the fugacity of sulfur (Toulmin and Barton, 1964). Many studies have utilized this pyrite-pyrrhotite relationship to understand sulfur and fluid systematics during ore body emplacement and regional and contact metamorphism and, in doing so, have observed a variety of metamorphic reactions that form pyrrhotite in natural systems (equations 1, 14, 19, 23, 26–28 in Table 3).

Pyrite and pyrrhotite are not the only iron minerals that undergo transformations and recrystallization during metamorphism. We compiled a comprehensive list of metamorphic reactions that involve iron-bearing minerals (Table 3), wherein each reaction denotes an eigenvalue in iron speciation space (Fig. 2). Vectors of arbitrary magnitude illustrate how metamorphic reactions can move iron between the Fe_{Py}, Fe_{HR}, and Fe_T pools in a range of directions; vector magnitude depends on reaction progress and protolith mineral assemblages. Reactions spanning low to high-grade metamorphism can skew iron speciation results toward and away from euxinic, ferruginous or oxic water column interpretations. Notably, some iron-bearing mineral phases only contain minor or trace amounts of iron which may not be captured by their general formulas (Table 2); inclusion of these phases would greatly expand the number of metamorphic reactions that could affect iron speciation. To quantitatively estimate the effect strength of these different reactions on iron mineralogy and speciation, we focused on several case examples from Paleozoic metasediments of the eastern United States.

5. METAMORPHIC CASE STUDIES

5.1. Site selection and geological background

We combed the literature for publications with detailed mineral assemblages of sedimentary rocks, with a focus on fine-grained siliciclastics, across metamorphic gradients. Due to the low-abundance of iron in shales (<7 wt%, e.g. Li and Schoonmaker, 2003), accessory minerals needed to be carefully tabulated as well, excluding normative XRF analyses. Many iron-bearing carbonates and silicates have variable stoichiometries, and therefore, analyses of mineral chemical compositions were needed for each mineral in each rock sample. Several hundred metamorphic petrology papers were evaluated, with ~30 publications fitting the criteria established above. We chose to examine two well-studied geologic locations: the metamorphosed Silurian-Devonian sedimentary rocks of the Connecticut Valley–Gaspé and the Central Maine troughs in the northern Appalachians (Osberg et al., 1989). These localities span from chlorite to kyanite zones; while most iron speciation studies have occurred on lower grade rocks, there is value in studying a broader range of metamorphism to learn how the proxy is affected by metamorphic processes. It is important to note that the sedimentary protoliths of these rocks were deposited as interbedded sandstones, shales, and carbonates in Paleozoic coastal marine settings; the depositional paleoenvironments for these settings is interpreted to be oxic (at least at the seafloor) based on the diverse faunal and floral assemblages of less metamorphosed stratigraphic equivalents (brachiopods, ostracodes, corals, sponges, echinoderms, calcareous algae) (e.g. Boucot, 1973; Copper, 2002; Denkler and Harris, 1988; Hughson and Stearn, 1988; Warshauer and Smosna, 1977; Watkins, 1996).

5.1.1. Waits River and Gile Mountain Formations, Vermont

The Waits River and Gile Mountain Formations in the Connecticut Valley-Gaspé Trough in Vermont present a classic case of the Barrovian metamorphic series spanning from the chlorite to the kyanite zone (Doll et al., 1961; Ferry, 1994). The Waits River Formation is composed predominately of tan siliceous limestone interbedded with calcareous organic-rich shales, while the overlying Gile Mountain Formation contains grey sandstones and shales with some interbedded black shales and rare carbonate beds (Fisher and Karabinos, 1980; Hatch, 1988; Lyons, 1955; Woodland, 1977). Bedding in both formations is on the centimeter to decimeter scale (Fisher and Karabinos, 1980). The sequence was deposited in Silurian through early Devonian time, based on dike, tuff, and detrital zircon ages (Hueber et al., 1990; McWilliams et al., 2010; Rankin and Tucker, 2009). The Waits River Formation contains crinoids and other echinoderm fragments and Devonian plant fossils are found in the Gile Mountain Formation (Hueber et al., 1990). The Waits River and Gile Mountain

Table 3
Example metamorphic reactions that transfer iron between pools.[a]

Eq.	Equation[b]	Lithology	Locality or model-system[c]	Zone	Fe_{HR}/Fe_T[d]	Fe_{py}/Fe_{HR}[d]		Ref.[e]
						Carb	Py	
1	$2py + CH_4 \rightarrow 2po + 2H_2S + C$	Graphitic pelite	Waterville	<Chlorite	–	↓	–	1
2	$2.689ms + 4.648pl + 1.99qz + 1.567dol + 0.029po + 0.03rt + 3.139CH_4 \rightarrow bt + 6.269pl + 1.6afs + 6.273C + 0.029H_2S + 7.937H_2O$	Graphitic pelite	Waterville	Biotite	↓	–	↓	1
3	$ms + 3qz + 8ank + 4H_2O \rightarrow 8cal + chl + bt + 8CO_2$	Calcareous pelite	Waterville & Sangerville-Vassalboro	Biotite	↓	–	–	2
4	$5ms + 8cal + 3chl + 7qz \rightarrow 5bt + 8pl + 12H_2O + 8CO_2$	Calcareous pelite	Waterville & Sangerville-Vassalboro	Biotite	↓	–	–	2
5	$2.77ms + 0.26ilm + 11.04ank + 1.86qz + 4.02H_2O + 0.08HCl \rightarrow chl + 2.83bt + 11.87cal + 10.21CO_2 + 0.08NaCl$	Carbonate	Sangerville-Vassalboro	Biotite	↓	–	–	3
6	$0.98ms + 2.23ank + 0.65qz + 0.09ilm + 0.03HCl + 0.01H_2O \rightarrow 1.09bt + 1.89cal + 0.48pl + 0.03NaCl + 2.57CO_2$	Carbonate	Sangerville-Vassalboro	Biotite	↓	–	–	3
7	$ms + 1.28cal + 0.84HCl \rightarrow 0.12bt + 0.02spn + 0.36qz + 1.22pl + 0.79KCl + 0.05NaCl + 1.30H_2O + 1.28CO_2$	Carbonate	Sangerville-Vassalboro	Biotite	↓	–	–	3
8	$ilm + 2cal + qz \rightarrow spn + ank$	Carbonate	Sangerville-Vassalboro	Biotite	–	–	–	4
9	$afs + 3po + 4H2O \rightarrow bt + 3H_2S$	Graphitic pelite	Waterville	Garnet	↓	–	↓	1
10	$0.560ms + 0.174chl + 1.080cal + 0.006ilm + 0.953HCl \rightarrow 0.190bt + 0.173grt + 0.394pl + 0.941qz + 1.080CO_2 + 1.541H_2O + 0.621NaCl + 0.332KCl$	Carbonate	Waterville	Garnet	↓	–	–	5
11	$5ank + 8qz + H_2O \rightarrow amp + cal + 7CO_2$	Carbonate	Waterville	Garnet	↓	–	–	6
12	$chl + 2.94cal + 5.73qz + 0.05ilm + 0.19pl \rightarrow 1.02amp + 0.86pl + 2.94CO_2 + 2.98H_2O$	Carbonate	Sangerville-Vassalboro	Amphibole	↓	–	–	3
13	$0.07amp + 0.59cal + 1.31pl + 0.01HCl + 0.59H2O \rightarrow zo + 0.002spn + 0.10qz + 0.01NaCl + 0.59CO_2 + 0.16H_2$	Carbonate	Sangerville-Vassalboro	Zoisite	↓	–	–	3
14	$2py + H_2O + C \rightarrow 2po + 2H_2S + CO_2$	Graphitic pelite	Waterville	Sillimanite	–	↓	–	1
15	$1.378ms + 0.049chl + 0.33qz + 0.485ank + 2.641sd + 0.340rt \rightarrow 1.492bt + 0.454pl + 0.254ilm + 3.162CO_2 + 0.082H_2O$	Pelite	Gile Mountain	Biotite	↓	–	–	7
16	$0.005ms + 0.052ank + 0.056pl + 0.002rt + 0.068CO_2 \rightarrow 0.172cal + 0.25qz + 0.005H_2O$	Carbonate	Gile Mountain	Biotite	↓	–	–	7
17	$1.021ms + 0.034chl + 1.497ank + 0.024rt + 1.573HCl \rightarrow 0.465bt + 0.225pl + 0.324grt + 1.579qz + 2.994CO_2 + 1.479H_2O + 1.139NaCl + 0.434KCl$	Psammite	Gile Mountain	Garnet	↓	–	–	5
18	$0.007bt + 0.119chl + 0.065ank + 0.078pl + 0.279qz \rightarrow 0.003ms + 0.252grt + 0.002ilm + 0.129CO_2 + 0.481H_2O$	Pelite	Waits River	Garnet	↓	–	–	5
19	$ilm + py \rightarrow 2po + rt + 0.5O_2$	Graphitic pelite	FTS-GCOHS	<Chlorite	–	↓	↑	8
20	$4py + 3CO_2 + CH_4 + H_2O \rightarrow 4sd + 8H_2S$	Graphitic pelite	NCKFMASH-S	Chlorite	–	↓	↓	9
21	$chl + 4hem \rightarrow cld + 4mag + 2qz + H_2O$	Fe-rich pelite	FASH	Chlorite	↑	–	–	10
22	$3chl \rightarrow 3alm + 2mag + 12H_2O (+QFM)$	Fe-rich pelite	FASH	Garnet	↑	–	–	10
23	$mag + 3py + 2C \rightarrow 6po + 2CO_2$	Carbonate	Orr Fm., UT	<Chlorite	–	↓	↑	11
24	$3sd + 0.5O_2 \rightarrow mag + 3CO_2$	Iron formation	Biwabik Fm., MN & Naugeene Fm., MI	Chlorite	–	–	–	12,13
25	$5.31ank + 8.75pg + 4.8po + 3.57pl + 16.83qz + 1.97O_2 \rightarrow grt + 16.44pl + 1.53chl + 2.4S_2 + 1.9H_2O + 10.62CO_2$	Pelite	Horsethief Creek Grp., British Columbia	Garnet	↓	–	↓	14
26	$bt + 3py + 1.5CH_4 \rightarrow afs + 6po + 4H_2O + 1.5C$	Graphitic pelite	Partridge and Paxton Fms., MA	Sillimanite	↑	↓	–	15
27	$ilm + H_2S \rightarrow rt + po + H_2O$	Graphitic pelite	Partridge and Paxton Fms., MA	Sillimanite	–	–	↑	15
28	$bt + 3H_2S \rightarrow afs + 3po + 4H_2O$	Graphitic pelite	Partridge and Paxton Fms., MA	Sillimanite	↑	–	↑	15
29	$2ank + 3qz \rightarrow di + opx + cal + 3CO_2$	Iron formation	Wabush Fm., Newfoundland	Kyanite	↓	–	–	16
30	$14ank + 16qz + H_2O \rightarrow tr + amp + 14cal + 14CO_2$	Iron formation	Wabush Fm., Newfoundland	Kyanite	↓	–	–	16

[a] The numerous reactions moving iron between poorly reactive silicate and unreactive silicate pools are not included in this sampling.

[b] Abbreviations for most minerals are listed in Table 2. Additional mineral abbreviations: dolomite = dol, siderite = sd, hematite = hem, magnetite = mag, chloritoid = cld, alm = almandine, orthopyroxene = opx, tremolite = tr. QFM means the quartz-fayalite-magnetite buffer.

[c] Abbreviations: $N = Na_2O$, $C = CaO$, $K = K_2O$, $F = FeO$, $M = MgO$, $T = TiO_2$, $S = SiO_2$, $A = Al_2O_3$, $H = H_2O$, -GCOHS = graphite saturated C-O-H-S fluids, $-S = H_2S$, Fm(s). = Formation(s), Grp. = Group, UT = Utah, MN = Minnesota, MI = Michigan, MA = Massachusetts

[d] Shows increase (up arrow), decrease (down arrow), or no change (–) in the iron speciation ratios Fe_{HR}/Fe_T and Fe_{py}/Fe_{HR} during the reaction progress with pyrrhotite in either Fe_{carb} or Fe_{py} pools.

[e] References: (1) Ferry (1981), (2) Ferry (1976b), (3) Ferry (1983a), (4) Ferry (1983b), (5) Ferry (1994), (6) Ferry (1979), (7) Ferry (1988b), (8) Connolly and Cesare (1993), (9) Tomkins (2010), (10) Bucher and Frey (2002), (11) Gillett (2003), (12) Jones (1972), (13) French (1973), (14) Haase (1982), (15) Tracy and Robinson (1988), (16) Klein (1966).

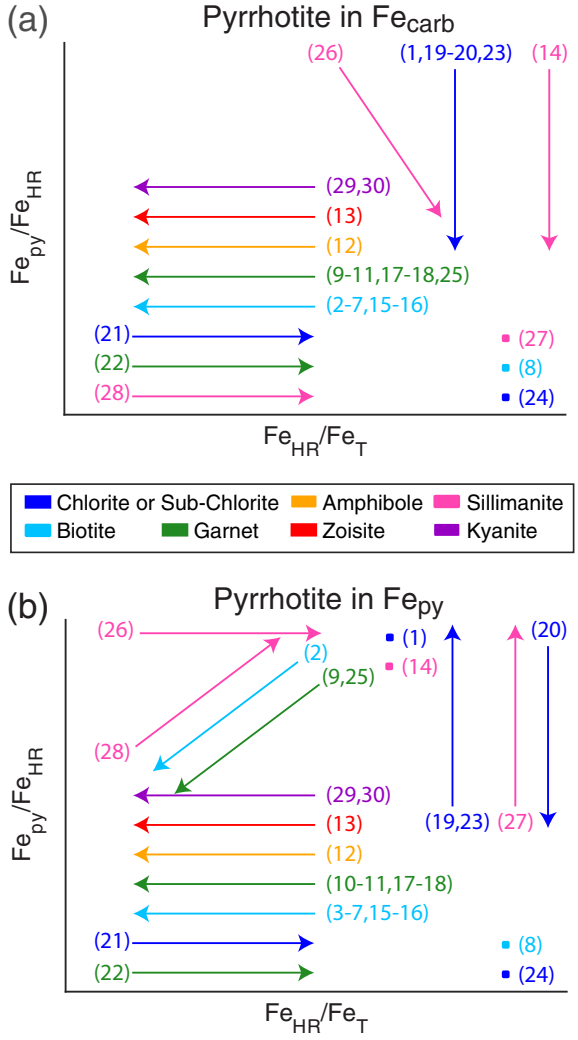

Fig. 2. Examples of known metamorphic reactions that transform iron between pools plotted in iron speciation place. Each vector shows the direction ratios will move in iron speciation space, given arbitrary reaction progress and mineral abundances. Vectors are color-coded by metamorphic zone when the reaction first occurs (cooler colors are lower metamorphic grade) with the same key for both plots. Numbers correspond to equations in Table 3 where more details on the reactions can be found. Two plots are shown: (a) for pyrrhotite placed in the Fe_{carb} pool, (b) for pyrrhotite in the pyrite pool (Fe_{py}). (For interpretation of the references to color in this figure legend, the reader is referred to the web version of this article.)

Formations were folded, intruded by granitic plutons, and then regionally metamorphosed during the Devonian Acadian orogeny (McWilliams et al., 2013; Osberg et al., 1989; Spear and Harrison, 1989; Thompson and Norton, 1968; Thompson et al., 1968). Mapped metamorphism of pelitic schist units spanned the chlorite through biotite, garnet, staurolite, and kyanite zones (Doll et al., 1961; Ferry, 1994); within the metamorphosed carbonate rocks of the Waits River Formation, isograds and zones were mapped based on the presence of ankerite, oligoclase, biotite, amphibole, and diopside (Ferry, 1992). Temperatures ranged from 400–450 °C in the chlorite zone with similar temperatures for the ankerite-albite zone up to 525–575 °C in the diopside and kyanite zones (Ferry, 1988b, 1992, 1994; Léger and Ferry, 1993). Pressure estimates varied from 3.5 to 7.8 kbar (Ferry, 1988b, 1992; Léger and Ferry, 1993). Two biotite-zone samples in this data set are from the neighboring Cambrian to Ordovician Albee-Dead River Formation, composed of thinly bedded greenish-grey shale with less common sandstone, which experienced similar metamorphic histories and P-T conditions as the nearby Gile Mountain Formation (Ferry, 1988b; Moench et al., 1995). Numerous studies have been performed on the metamorphism of the region with a focus on fluid infiltration (e.g. Ferry, 1988b; Léger and Ferry, 1993).

A total of 116 samples were assessed in our study from the Waits River, Gile Mountain, and Albee-Dead River Formations—82 metacarbonates, 12 psammites (metamorphosed quartz-rich siliclastics e.g. sandstones), and 20 pelites (metamorphosed fine-grained aluminous siliclastics e.g. claystones)—with mineral assemblages and mineral chemistry from Ferry (1988b, 1992, 1994, 2007), Léger and Ferry (1991, 1993), Penniston-Dorland and Ferry (2006, 2008). Sandstones might not be expected to record water-column redox conditions as precisely as shales (or carbonates) due to the coarser grain-size of detrital material. However, they represent part of the siliciclastic spectrum, include similar amounts of cements, and can provide an additional window into iron mobility during diagenesis and metamorphism; thus they were included in the analyses. Metamorphic grades of carbonate and pelitic isograds were ordered and correlated based on temperature estimates; note that the biotite zone in carbonates is approximately the same as the garnet zone in pelites and they have been grouped.

5.1.2. *Waterville and Sangerville-Vassalboro Formations, Maine*

The Waterville and Sangerville-Vassalboro Formations in the Central Maine Trough record a classic example of the metamorphic gradient following the Buchan series from the chlorite to the sillimanite zone (Osberg, 1968). The Waterville Formation is composed of thinly bedded greenish grey shale, black shale, and shaly sandstone with a shaly carbonate member while the overlying Sangerville-Vassalboro Formation is composed of interbedded gray shaly sandstones and carbonates with minor sulfidic black shales (Ferry, 1981, 1983b; Osberg, 1988; Osberg, 1968). Compositional layering occurs on the centimeter to decimeter scale (Ferry, 1981, 1983b). The sequence was deposited during the Silurian through Devonian as constrained by graptolite index fossils, detrital zircons, and subsequent granitic intrusions (Ludman, 2014; Osberg, 1968; Pankiwskyj et al., 1976; Tucker et al., 2001). The ~380 Ma intrusions occurred after structural deformation of the Waterville-Sangerville-Vassalboro Formations, and then the entire package was subjected to regional metamorphism during the Devonian Acadian orogeny (Osberg, 1988; Tucker et al., 2001; Wing et al., 2003). Metamorphic isograds were mapped in the pelitic schists spanning the biotite, garnet, staurolite-andalusite, and sillimanite zones, approximately perpendicular to bedding (Osberg, 1968).

Isograds in the metacarbonate rocks were also noted from appearances of biotite-chlorite, amphibole-anorthite, zoisite, microcline-amphibole, diopside, and scapolite in increasingly higher grade rocks; these isograds are mapped directly on top of the pelitic isograds so direct comparison is possible (Ferry, 1976b). Pressure conditions during metamorphism were estimated at 3.5 kbar with temperatures ranging from 380 °C at the biotite isograd to 550 °C in the sillimanite zone (Ferry, 1976a, 1980). Numerous studies highlighted the open system nature of regional metamorphic reactions with fluid infiltration of the rock package (e.g. Ferry, 1988a; Penniston-Dorland and Ferry, 2006).

A total of 52 samples were utilized in our study from the Waterville and Sangerville-Vassalboro Formations—35 metacarbonates, 9 psammites, and 8 pelites—with mineral assemblages and mineral chemistry from Ferry (1976b, 1984, 1988a, 1994), and Penniston-Dorland and Ferry (2006). Lithology was poorly denoted within some papers due to analysis of impure carbonates (Ferry, 1976b, 1988a), so classification of samples as pelite versus psammite versus carbonate was made based on the modal volume ratio of micas or carbonates to quartz (<25% cut off for pelite or carbonate) and/or the elemental ratio of $Al_2O_3/CaO/SiO_2$, as per Bickle et al. (1997). Metamorphic grade of carbonate and pelitic isograds was correlated and combined based on the isograd map of the locality from Ferry (1976b) and Ferry (1994) with pelitic schist terminology preferred if there were approximately equivalent metamorphic zones.

5.2. Data reduction

For the two targeted localities above, we used the data on iron-bearing minerals to calculate the samples' iron speciation Fe_{HR}/Fe_T and Fe_{py}/Fe_{HR} ratios. These results were paired with information about the sample lithology and metamorphic zone to understand how progressive metamorphism affects iron speciation results. In order to take the published literature data and use it to find Fe_{HR}/Fe_T and Fe_{py}/Fe_{HR} ratios, several processing steps were required.

Mineral assemblages are presented in the literature as modal volume percentages or moles per liter rock based on point counting minerals in thin section (typically 2000 points). For the former, volume percent was converted to molar amount per liter rock using molar volume data from Robie et al. (1967) and Holland and Powell (1998). Hexagonal pyrrhotite's molar volume was used, and molar volumes of micas, garnet, allanite, tourmaline, and amphiboles were found by averaging endmembers. In some trace minerals (less than 0.05 vol%), the exact abundance of a mineral was not quantified, simply absence or presence. If presence was marked, we calculated molar amount per liter rock based on the maximum abundance (0.05 vol%) as well as for the minimal abundance (0 vol%). Overall, these two treatments of trace minerals did not affect the results significantly; however, the change was noticeable in Fe_{py}/Fe_{HR} due to the low abundance of sulfide-bearing phases in many samples (Figs. EA-1–EA-4). All further calculations of iron speciation ratios and discussion in the main text and supplement include the trace minerals and can be treated as a maximum. Although data were selected carefully to make sure trace minerals were counted, it is possible that iron from certain phases was underrepresented by the point counting technique due to small grain size or domains within larger minerals, which could affect our calculations of Fe_{HR}/Fe_T and Fe_{py}/Fe_{HR} ratios.

The amount of iron in 1 liter of rock was calculated by multiplying the moles of a mineral by the iron content within the mineral based on its formula. The mineral formula was calculated based on the published average electron microprobe analyses for each mineral, based on more than one spot per grain and more than one grain within a given sample/thin section. If the mineral composition was not precisely published for a given sample, the average from other samples within the publication at the same metamorphic grade and/or same lithology was used. If this was not possible, the average for the mineral within the publication was used. When no mineral composition data was reported, standard formulas were used (Table 2). Utilizing the mineralogical iron pool assignments in Table 2, non-dimensional ratios of Fe_{py}/Fe_{HR} and Fe_{HR}/Fe_T could be calculated and are presented in Figs. 3–6 and EA-5–EA-6.

6. RESULTS

A wide range of Fe_{py}/Fe_{HR} and Fe_{HR}/Fe_T ratios were found from the data of the Waits River, Gile Mountain, Waterville, and Sangerville-Vassalboro Formations, which might be taken to indicate variably oxic, ferruginous, and euxinic water column conditions using the iron speciation proxy (Figs. 3 and 4). As mentioned above, based on fossil assemblages, it is reasonable to infer that these rocks were deposited under conditions sufficiently oxic to support the metabolisms of a diverse metazoan benthic community; several post-depositional factors could contribute to the high ratios of Fe_{py}/Fe_{HR} and Fe_{HR}/Fe_T. Through more detailed plots to look at trends by lithology and metamorphic zone (Figs. 5 and 6, EA-5, EA-6) as well as the mineral data itself (Figs. 7, EA-7), we noted similar trends and ratios between the two locations suggesting some basic fundamental processes. The statistical significance of all trends discussed in the text was quantified for the more numerous Vermont samples using a two-sample t-test for population comparison and nonparametric Mann–Kendall Test for trend analysis (Tables EA-1 and EA-2). We were able to untangle some of the causes changing Fe_{py}/Fe_{HR} and Fe_{HR}/Fe_T and discuss the importance of these in actual iron speciation experiments below.

7. DISCUSSION

7.1. Pyrrhotite pool placement

One of the largest differences in the ratio results was determined by which pool pyrrhotite was assigned, either Fe_{carb} or Fe_{py} (Figs. 3 and 4). The Fe_{HR}/Fe_T ratios were not affected since pyrite and carbonate are both highly reactive species and therefore included in Fe_{HR}. However,

Fe_{py}/Fe_{HR} was significantly increased due to the additional pyrrhotite fraction in Fe_{py} (Figs. 6, EA-6). In the metasedimentary rocks studied here, pyrrhotite was in general more common than other iron sulfides (pyrite or chalcopyrite) across all zones. The addition of pyrrhotite to the Fe_{py} pool was enough to push Fe_{py}/Fe_{HR} ratios above 0.8, into the zone of euxinic conditions, in some of the carbonates and a sandstone from the Vermont and Maine localities.

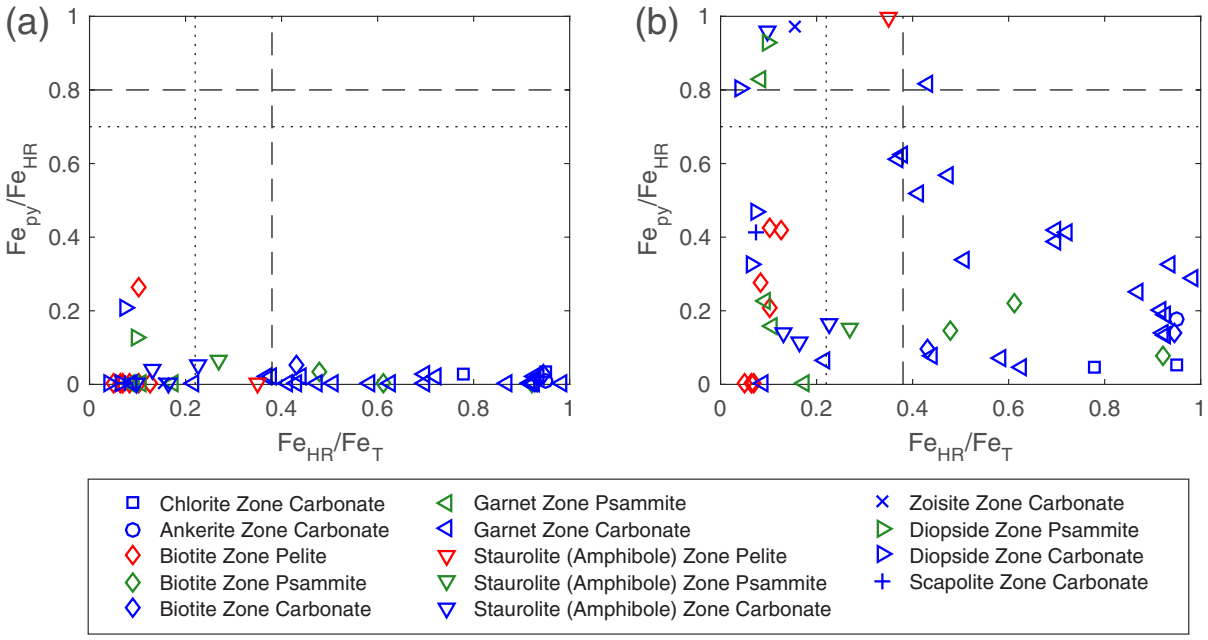

Fig. 3. Waterville and Sangerville-Vassalboro Formations data plotted in iron speciation space. Legend is the same for both plots with different symbols representing the 8 different metamorphic zones color-coded by lithology. Staurolite (Amphibole) stands for the pelitic schist and carbonate facies respectively. (a) Pyrrhotite in the Fe_{carb} pool. (b) Pyrrhotite in the pyrite pool (Fe_{py}). Figs. EA-5 and EA-6 show expanded plots for more detail. (For interpretation of the references to color in this figure legend, the reader is referred to the web version of this article.)

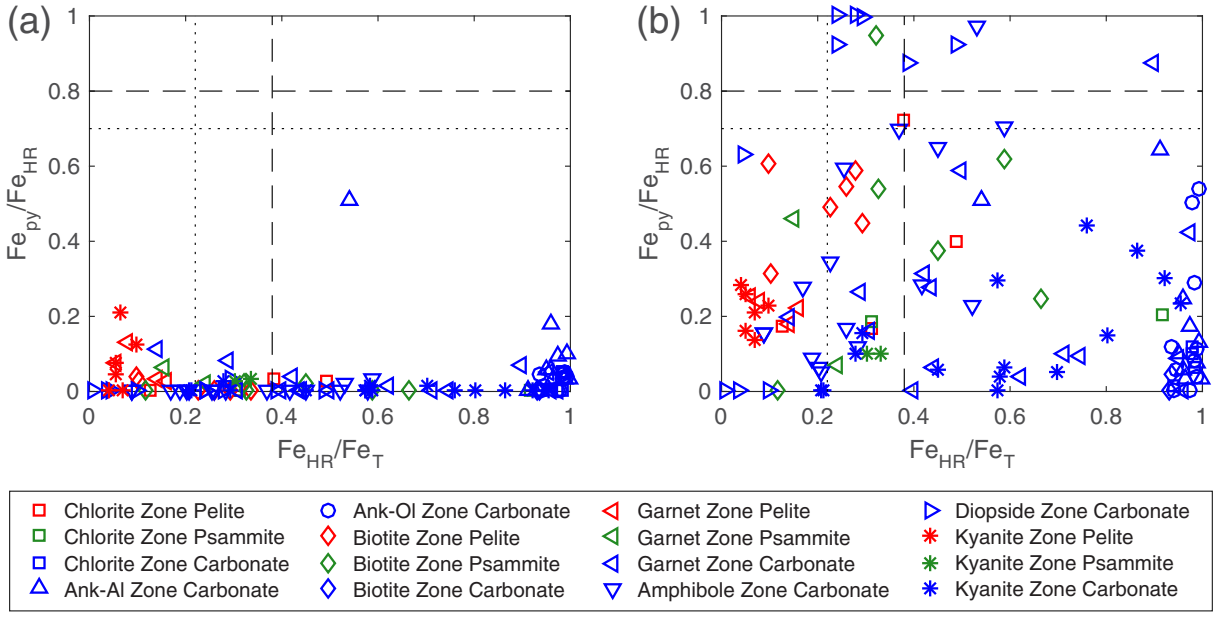

Fig. 4. Waits River and Gile Mountain Formations data plotted in iron speciation space. Legend is the same for both plots with different symbols representing the 8 different metamorphic zones color-coded by lithology. Ank-Al stands for Ankerite-Albite and Ank-Ol stands for Ankerite-Oligoclase. (a) Pyrrhotite in the iron carbonate (Fe_{carb}) pool. (b) Pyrrhotite in the pyrite pool (Fe_{py}). Fe_{py}/Fe_{HR} is the ratio of pyrite to highly reactive iron and Fe_{HR}/Fe_T is the ratio of highly reactive to total iron. Figs. 5 and 6 show expanded plots for more detail. (For interpretation of the references to color in this figure legend, the reader is referred to the web version of this article.)

Therefore, if pyrrhotite is included in Fe_{carb} as in older studies or through misdiagnosis of the mineral assemblage, the samples will appear much more ferruginous than they would otherwise. Prior analyses on pelites from the Waterville Formation suggest a direct transformation of iron in pyrite into pyrrhotite due to a progressive loss of sulfur (Ferry, 1981). On the other hand, pyrrhotite can form from the decomposition of iron oxides and iron silicates even at low-metamorphic grade (<200 °C) upon interaction with H_2S-bearing fluids or co-decomposition of pyrite (Gillett, 2003; Hall, 1986; Nesbitt and Kelly, 1980; Tracy and Robinson, 1988). In these circumstances, placing pyrrhotite in the Fe_{py} pool will drive iron speciation ratios toward the euxinic zone. Careful petrographic study of the pyrrhotite could help determine which reaction scenario is the case through pseudomorphs, rims, or partially reacted phases (e.g. Zhou et al., 1995). Additional isotopic study could help determine the importance of S-rich fluids (e.g. Gillett, 2003), although determining "background" or "normal" can be difficult in ancient, relatively metamorphosed samples. Mineral assemblages could give clues as well, but often clear-cut metamorphic grades cannot be or are not sampled. Because of these complications, the simplest solution may be to screen and avoid samples containing pyrrhotite for iron speciation work.

7.2. Lithological controls and diagenesis

An important control on iron speciation ratios is the lithology of the samples. To a certain degree, it is not surprising that different lithologies might reflect differing redox conditions upon deposition, e.g. sandstones and siltstones reflect nearer-shore environments with more detrital inputs and shallower waters than shales and carbonates (Walker and James, 1992). However, fine-scale intercalation of these lithotypes at the scale of bedding is observed within all of the formations studied here (e.g. Ferry, 1994). Thus the variation seen in iron speciation proxy estimates for these formations is more a product of lithotype (including mineralogy and subsequent metamorphism) than it is paleoenvironment.

Lithological differences were most noticeable in Fe_{HR}/Fe_T, where pelites had much lower values and a smaller range than psammites and carbonates of the same formation regardless of metamorphic zone (Figs. 5a, EA-5a). Even if samples only were examined at the lowest metamorphic grades (chlorite, ankerite, biotite) to separate lithological distinctions from metamorphic processes, pelites had low Fe_{HR}/Fe_T ratios compared to the carbonates and psammites at the same metamorphic grade (Figs. 5b–d, EA-5b–d).

By examining the results of the calculations in the context of the mineralogy, it is apparent that the primary reason for the differences between lithologies was the abundance of iron in carbonates either as minor components in calcite or as ankerite (Figs. 7d, EA-7d). Almost all of the psammites studied here included some carbonate minerals while the pelites had much lower amounts of carbonate. Although previous geochemical work suggested that carbonate-rich samples behave in the Fe_{HR}/Fe_T proxy similarly to siliciclastic samples (Clarkson et al., 2014), this work was performed on modern carbonates with minimal diagenetic overprints. Iron can be incorporated into carbonates in primary precipitates; however, in modern oxygenated waters, soluble iron contents are very low, so most iron is incorporated in carbonates through early or secondary diagenetic cements formed in anoxic pore fluids (Barnaby and Rimstidt, 1989; French, 1973; Warren, 2000). Some of this iron could be sourced from the original highly-reactive iron pool, but it is not guaranteed due various formation reactions and open-system processes. These diagenetic overprints could dominate the Fe_{HR}/Fe_T signals in Phanerozoic and Precambrian carbonate rocks enough to cause erroneous paleoredox interpretations for the water column. Notably, in the data analyzed here, the large Fe_{carb}

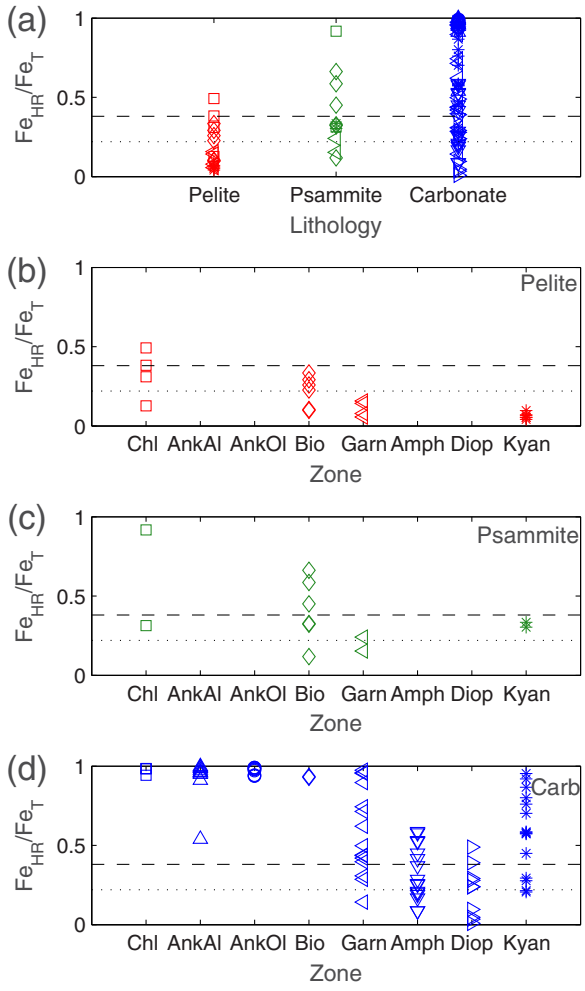

Fig. 5. Highly reactive iron to total iron (Fe_{HR}/Fe_T) ratios in detail separated by lithology and zone for Waits River and Gile Mountain Formations. Same symbols as Fig. 4; here labeled on the plots with symbols for metamorphic zone color-coded by lithology. Abbreviations are: Chl = Chlorite, Ank-Al = Ankerite–Albite, Ank-Ol = Ankerite-Oligoclase, Bio = Biotite, Amph = Amphibole, Diop = Diopside, Kyan = Kyanite, Carb = Carbonate. (For interpretation of the references to color in this figure legend, the reader is referred to the web version of this article.)

pool was not simply due to the presence of ankerite in samples, which has been suggested as a screening method for diagenetic alteration before doing iron speciation (Clarkson et al., 2014). In fact, trace amounts of iron in calcite constituted over 50% of the Fe_{carb} pool in almost all of the low-grade carbonates due to the abundance of this phase, and samples with low abundances of ankerite still had high Fe_{HR}/Fe_T within the limits indicating anoxia. In contrast, more of the iron in the Fe_{carb} pool of low-grade psammites usually came from ankerite, and its presence in siliciclastics could be a better signal for diagenetic alteration. Overall, samples with proportionately large Fe_{carb} pools should be investigated petrographically to determine whether the carbonates comprise elements of the primary sediment or rather reflect diagenetic/metamorphic cements.

At low-metamorphic grades, Fe_{py}/Fe_{HR} was generally higher in pelites than in psammites and carbonates (Figs. 6b–d, EA-6b–d), especially when pyrrhotite was included in the Fe_{py} pool (Figs. 6f–h, EA-6f–h). The observation was also expected from common early diagenetic reactions. Although pyrite can form within the water column (Raiswell and Berner, 1985; Wilkin and Barnes, 1997), it more commonly forms in sediments underlying oxic and sub-oxic waters through scavenging of highly-reactive iron in pore waters that are anoxic and sulfide-rich (Berner, 1970; Canfield and Berner, 1987; Wilkin et al., 1996). Due to their high organic contents and slow depositional rate, shales are more likely to form early diagenetic pyrite than sandstones or carbonates (e.g. Berner, 1984; Curtis, 1978). Although low-grade pelites had higher Fe_{py}/Fe_{HR} ratios than other lithologies, generally these higher ratios did not fall within the limits for euxinic conditions, suggesting the iron speciation proxy is less sensitive to this sort of diagenetic alteration.

7.3. Increasing grade and metamorphic reactions

The detailed breakdown of the Fe_{HR}/Fe_T and Fe_{py}/Fe_{HR} ratios by metamorphic zone highlighted trends that occur with increasing metamorphic grade

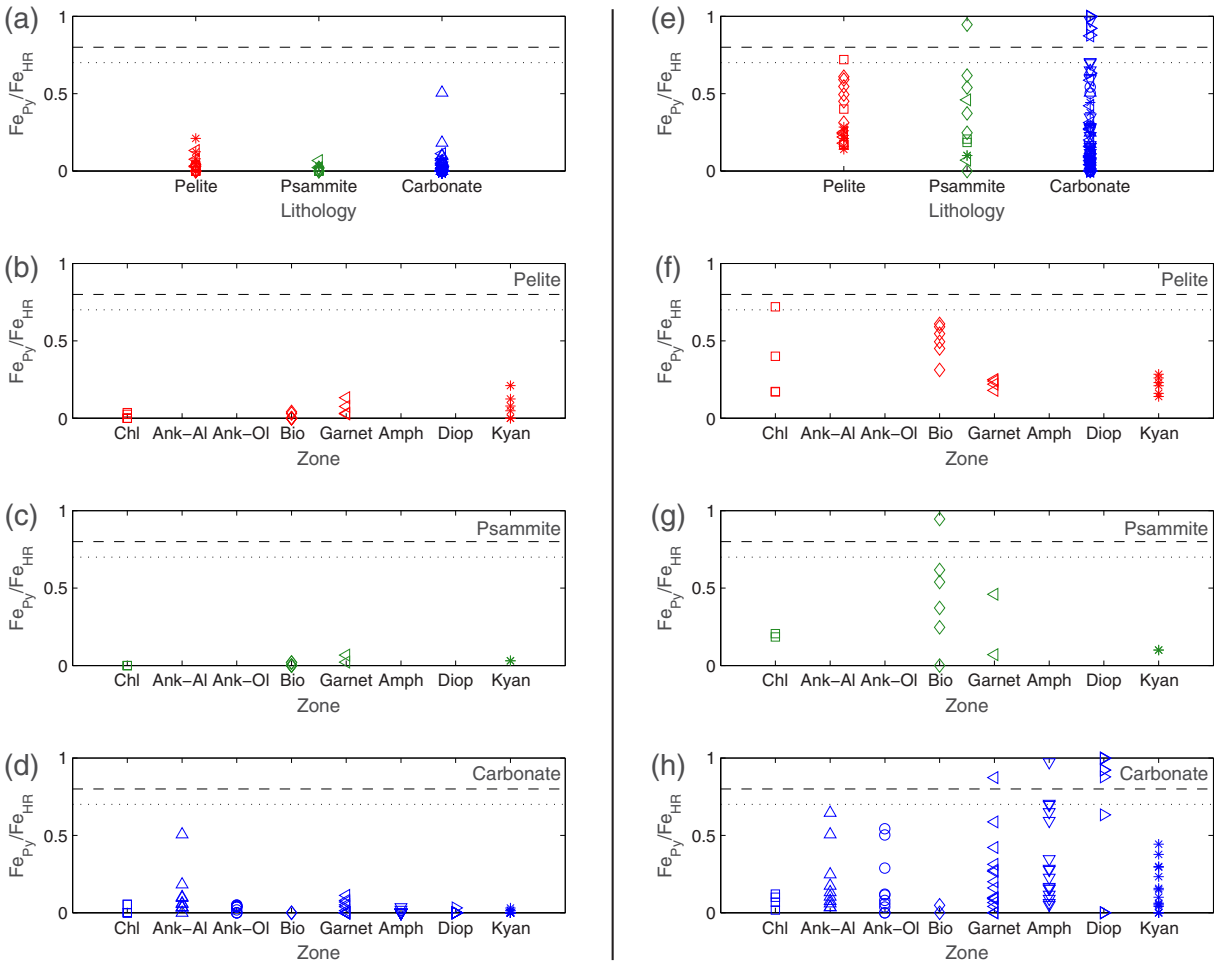

Fig. 6. Pyrite to highly reactive iron (Fe_{py}/Fe_{HR}) ratios in detail separated by lithology and zone for Waits River and Gile Mountain Formations. (a–d) Pyrrhotite in the iron carbonate (Fe_{carb}) pool. (e–h) Pyrrhotite in the Fe_{py} pool. Same symbols as Fig. 4; here labeled on the plots with symbols for metamorphic zone color-coded by lithology. Abbreviations for zones are: Chl = Chlorite, Ank-Al = Ankerite–Albite, Ank-Ol = Ankerite-Oligoclase, Bio = Biotite, Amph = Amphibole, Diop = Diopside, Kyan = Kyanite. (For interpretation of the references to color in this figure legend, the reader is referred to the web version of this article.)

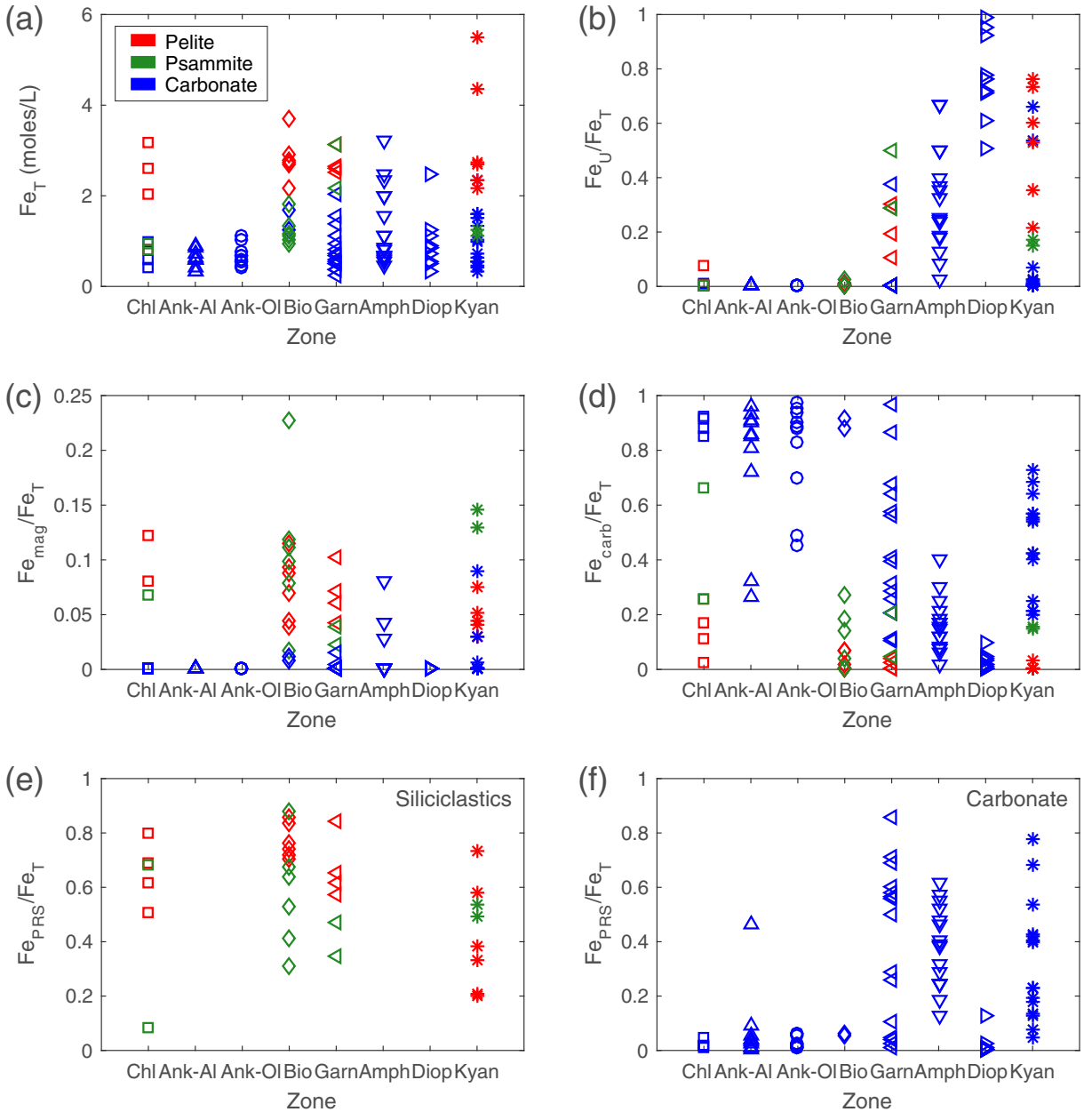

Fig. 7. Different iron pools separated by metamorphic grade in samples from Waits River and Gile Mountain Formations. (a) Total iron (Fe_T). (b) Ratio of unreactive silicate iron to total iron (Fe_U/Fe_T). (c) Ratio of magnetite iron pool (entirely ilmenite here) to total iron (Fe_{mag}/Fe_T). Note this is at a different scale than (b–f). (d) Ratio of carbonate iron to total iron (Fe_{carb}/Fe_T). (e) Ratio of poorly reactive sheet silicates to total iron (Fe_{PRS}/Fe_T) for pelites and psammites. (f) Ratio of poorly reactive sheet silicates to total iron (Fe_{PRS}/Fe_T) for carbonate. Same symbols as Fig. 4; lithology color codes in legend in (a) with symbols for metamorphic zone labeled on plots. Abbreviations for zones are: Chl = Chlorite, Ank-Al = Ankerite–Albite, Ank-Ol = Ankerite-Oligoclase, Bio = Biotite, Garn = Garnet, Amph = Amphibole, Diop = Diopside, Kyan = Kyanite. All data here is assuming pyrrhotite is in the pyrite pool (Fe_{py}). (For interpretation of the references to color in this figure legend, the reader is referred to the web version of this article.)

(Figs. 5 and 6, EA-5, EA-6). These ratio changes of Fe_{HR}/Fe_T and Fe_{py}/Fe_{HR} were due to movement of iron between different pools during progressive metamorphism; however, for each ratio, we needed to determine which of the two pools was changing in size (or whether both were changing). Total iron did not vary systematically with metamorphic grade, although it did by lithology (Figs. 7a, EA-7a), suggesting that these metamorphic systems were mostly closed with respect to iron although open with respect to fluids carrying C-O-H-S and other elements (e.g. Ferry, 1981, 1983b, 1988b). Therefore, the individual pools were normalized by total iron for comparison purposes. Additionally, changes in Fe_{carb}, Fe_{mag}, Fe_{py}, Fe_{PRS}, and Fe_U could occur due to changes in abundances of minerals or due to changes in mineral composition with loss or addition of iron; we did not distinguish between

these options, although it appeared that abundance variation played a larger role since iron compositions of minerals did not vary greatly across metamorphic zones within the data analyzed here. The one possible exception was ankerite, which on average may have lost iron with increasing metamorphic grade in some studies (e.g. Waits River Formation, Ferry (1992) and Waterville Formation, Ferry (1994)).

Fe_{HR}/Fe_T in general decreased with increasing grade, although slight differences were seen between the siliciclastic and carbonate samples (Figs. 5b–d, EA-5b–d). While a more monotonic decrease was seen in siliciclastics starting from the chlorite zone, the decrease in carbonates occurred only after the garnet zone. The kyanite zone carbonates of the Waits River Formation with the highest P-T conditions in either locality (Ferry, 1994; Penniston-Dorland and Ferry, 2006) showed a return to previous values. The main driver for ratio changes appeared to be variation in the Fe_{carb} pool, (specifically of the iron carbonates, not pyrrhotite) as changes in Fe_{carb} mirror the trends described above even including the upswing in kyanite zone carbonates (Figs. 7d, EA-7d). There was an inverse correlation with these changes in the Fe_U pool suggesting that the metamorphic growth of silicates containing iron such as garnet and amphibole utilized iron from iron carbonates (Figs. 7b, EA-7b).

Fe_{py}/Fe_{HR} displayed more complex behavior with increasing metamorphism and effects were separated by lithology (Figs. 6, EA-6). Chalcopyrite and pyrite did not change in fraction very much across metamorphic zones; therefore, large changes in Fe_{py}/Fe_{HR} were controlled by pyrrhotite or other minerals in the Fe_{HR} pool. When pyrrhotite was excluded from the Fe_{py} pool, a slight decreasing trend was resolved in the carbonate samples. In pelitic and psammitic samples, a slight increase in Fe_{py}/Fe_{HR} occurred with metamorphic grade apparently due to decreases in the rest of the Fe_{HR} pools. When pyrrhotite was included in the Fe_{py} pool, psammites exhibited no trend probably due to the low number of samples; a few samples did show high Fe_{py}/Fe_{HR} ratios within the euxinic limits at high(er) metamorphic grades. In pelites, when pyrrhotite was included in the Fe_{py} pool, a decrease in Fe_{py}/Fe_{HR} was observed due to significant decreases in pyrrhotite after the biotite zone. In carbonate samples, when pyrrhotite was included in the Fe_{py} pool, values for Fe_{py}/Fe_{HR} for carbonates increased with increasing metamorphic grade such that some samples fell within the limits for euxinic redox conditions at high grades. Pyrrhotite increased slightly with metamorphic grade (on average) in carbonates, which combined with the decrease of the Fe_{HR} pool increased the Fe_{py}/Fe_{HR} ratio. Notably, the highest-grade samples from the kyanite and scapolite zones showed a decrease in Fe_{py}/Fe_{HR} probably due to increases in the Fe_{HR} pool discussed above. Based on detailed analysis of the raw data, pyrrhotite formation might also have been dependent on lithological differences or local fluid flow conditions as certain sites had higher pyrrhotite abundances than other sites at the same metamorphic grade.

Although Fe_{PRS} was at times a significant part of the total iron pool, the poorly reactive sheet silicates did not appear to drive Fe_{HR} or Fe_T to any substantial degree and trends differed between sites and within sites between lithologies (Figs. 7ef, EA-7ef). Metamorphically, this suggests that several reactions exist forming and destroying distinct micas and chlorite across metamorphic grades utilizing different reactants and/or that multiple poorly reactive silicate minerals are involved in reactions adding complexity; within carbonates, iron may come from iron carbonates for the formation of biotite and transfer upon destruction to help form unreactive silicates (or pyrrhotite) while siliciclastic rocks may have more internal cycling of iron within the Fe_{PRS} pool. It is interesting that some of the iron transitions are fairly abrupt, such as biotite formation in Vermont carbonates at the garnet zone (Fig. 7f), whereas others, such as the slow decrease in the amount of biotite in Maine with metamorphic grade (Figs. EA-7ef), occur progressively across increasing metamorphic regimes.

The Fe_{mag} pool only contained ilmenite in this study and overall is a relatively small amount of the Fe_T pool—this is particularly the case in carbonates. Therefore, changes in ilmenite did not significantly affect the Fe_{HR}/Fe_T ratios, but did show interesting trends with metamorphic implications. Within carbonates, ilmenite varied similarly to unreactive silicate phases increasing at the garnet zone, while in pelites, it decreased, transforming slowly through metamorphism—a behavior similar to other highly-reactive iron phases (Figs. 7c, EA-7c).

Prior work on the Waits River, Gile Mountain, Waterville, and Sangerville-Vassalboro Formations proposed various metamorphic reactions based on analysis of mineral assemblages and thermodynamic calculations (Table 3, Fig. 2); the trends and shifts described above corresponded well with these reactions. The distinct metamorphic changes based on lithology and comparison of iron speciation results color-coded by lithology versus metamorphic grade (Figs. 3 and 4, EA-8, and EA-9) suggest that for this study, lithology was a more important control on the iron speciation ratios than metamorphic grade.

8. IMPLICATIONS

Our analysis using petrologic information of Paleozoic strata from New England emphasized a few of the issues that could impact interpretations of iron speciation paleoredox data generated from metamorphosed samples; the most important of these concern: (1) presence of pyrrhotite (2) genesis and behavior of iron carbonates and (3) metamorphic grade. Although most early iron speciation studies did not screen for pyrrhotite or AVS, this has become a more standard practice now and many studies note very low or no detectable AVS in their samples (e.g. Dickson et al., 2014; Gilleaudeau and Kah, 2015; Johnston et al., 2012; Och et al., 2016; Planavsky et al., 2011; Sperling et al., 2013). However, when pyrrhotite is detected, the analysis and interpretations that follow vary. Poulton et al. (2010) noted the presence of AVS in some of the analyzed samples, but used the Fe_{carb} pool to represent pyrrhotite (due to concerns about double-counting) and made no corrections for Fe_{py}. One potential issue with this technique

is that about 40% of these samples had significantly more Fe_{AVS} than Fe_{carb}. Additionally, the AVS/pyrrhotite only occurred in 3 out of 6 of the cores which represent the shallow facies separated by >100 km from the other higher-grade cores representing deeper facies. The presence of AVS/pyrrhotite could be highlighting differences in lithology or metamorphism between the cores that could skew the redox results; notably, most of the euxinic redox results occurred in these AVS-bearing cores. Taking the opposite approach, Reuschel et al. (2012) added Fe_{AVS} to the Fe_{py} pool and did not include the Fe_{carb} extraction in Fe_{HR}; this sulfide grouping was supported by analysis of iron speciation ratios and petrographic relations suggesting pyrrhotite formed from desulfurization of pyrite for the majority of their samples. However, they also noted that an external iron supply probably formed pyrrhotite and other iron minerals in a few samples at the top of their section with the overall effect of dampening the Fe_{HR}/Fe_T signal. Partin et al. (2015) petrographically described that pyrrhotite was prevalent throughout their samples, elected to group it with Fe_{py} (assuming both were quantitatively extracted during the CRS extraction), and treat Fe_{py} as a minimum since no stoichiometric calculations were performed to correct for pyrrhotite. However, they also noted that pyrrhotite was commonly associated with hematite and appeared to be forming at the expense of iron oxides as well as pyrite; if this occurred in a closed system, this reaction moved iron from the highly reactive pool to the pyrite pool, pushing iron speciation results toward euxinia. In an innovative approach, Asael et al. (2013) noted AVS/pyrrhotite which they interpreted to be from metamorphic overprinting and utilized the iron speciation to understand the metamorphic reaction (desulfurization). Samples affected by pyrrhotization were cautiously corrected based on other paired redox-proxies and excluded from further interpretations. Pyrrhotite formation is difficult to untangle without additional petrographic or field observations—it is probably best practice to just avoid samples and regions where this type of metamorphism has occurred.

Many iron speciation analyses have been performed on samples where the majority of the iron was held by carbonate phases (e.g. Canfield et al., 2008; Clarkson et al., 2016; Geboy et al., 2013; Izon et al., 2017; Johnston et al., 2013; Johnston et al., 2010; Li et al., 2015; Planavsky et al., 2011; Sperling et al., 2015; Wood et al., 2015) or where carbonate was the dominate pool of highly reactive iron (e.g. Canfield et al., 2007; El Albani et al., 2010; Farrell et al., 2013; Jin et al., 2016; Och et al., 2013; Poulton et al., 2010; Sperling et al., 2014; Sperling et al., 2013), giving ferruginous or ferruginous and oxic iron speciation results respectively. To evaluate the accuracy of the redox interpretation, it is valuable to consider that iron-rich carbonates often form as cements and from recrystallization of pre-existing carbonate phases during diagenesis and metamorphism. Several studies have drawn upon or considered this inference. Farrell et al. (2013) noted that the highest Fe_{HR} values were observed in siltstone beds and in concretions versus in mudstones and attribute these to late stages of early diagenesis while moderate values falling in the boundary zone between anoxic & oxic were attributed to dysoxic deep waters and anoxic pore waters. Li et al. (2015) noticed a strong linear correlation between weight percent total inorganic carbon (TIC) and the $Fe_{HR}/Fe_{T\ ratios}$ (linear and exponential correlations were seen between TIC and Fe_{carb}/Fe_T); although the authors noted that the iron speciation proxy seemed to be recording variations in detrital versus early diagenetic mineral abundance and that field relations showed early to mid-diagenetic carbonate precipitation, the study still concluded that the samples record ferruginous deep waters. Because iron carbonates play such an important role in iron speciation data generated on a diversity of sedimentary rocks, one simple and straightforward way to evaluate the petrogenesis of iron carbonates is by petrographic study, coupled with microprobe or chemical imaging analyses, on a subset of samples. This approach can readily assay the presence and abundance of iron in primary sedimentary grains or instead illustrate that these phases reflect diagenetic (or even metamorphic) cements and textures (Scholle and Ulmer-Scholle, 2003). Isotopic analyses, both in situ and bulk, can provide an additional window into understanding the paragenesis and modification of carbonate minerals, including cements.

Although most iron speciation studies have focused on sub-greenschist facies rocks, metamorphic reactions and fluid flow can still occur at these low-temperatures (e.g. <250C)—engendering geochemical and mineralogical processes that affect iron speciation. To build a more continuous iron speciation record through Proterozoic time, some studies have started to analyze rocks that have been metamorphosed to greenschist facies or above. Asael et al. (2013) and Partin et al. (2015) both worked on ~2.0–1.9 Ga greenschist facies rocks (with the latter study extending to lower amphibolite facies) that contained prevalent pyrrhotite interpreted to form metamorphically from pyrite (Melezhik et al., 2015; Partin et al., 2014). As discussed above, through the use of petrography and iron speciation extractions, the metamorphic reactions were respectively attributed to open system fluid desulfurization reactions and closed system iron oxide sulfurization from neighboring pyrite. Partin et al. (2015) also noted the presence of biotite locally overgrowing pyrrhotite, which suggested some repartitioning of highly reactive and pyrite iron into the poorly-reactive sheet silicate pool; however, this was not addressed further in the study. The Poulton et al. (2010) study on ~1.8–1.9 Ga sub-greenschist to lower greenschist facies rocks found many samples with Fe_{HR}/Fe_T values in the nebulous oxic or anoxic region between limits and suggested this was due to either rapid sedimentation, increase in tuffaceous input, or the transformation of oxides and carbonates into clay minerals during burial diagenesis/metamorphism; in many of these samples, the proportion of Fe_{PRS}/Fe_T was much higher than the Phanerozoic average leading to the conclusion that post-depositional formation of clay minerals did indeed lower the original Fe_{HR}/Fe_T. Based on results from another redox proxy (Fe_T/Al), the study concluded the sediments were deposited in ferruginous waters even those with subdued Fe_{HR}/Fe_T ratios. In general, iron speciation studies on obviously altered rocks do a good job at carefully analyzing post-depositional overprints, but more rarely adjust their

data and interpretations for the style of alteration observed. Our results illustrate that it is possible to model primary mineralogy from a metamorphic assemblage as long as detailed quantitative petrographic and chemical measurements are made following the sorts of petrographic techniques commonly applied by metamorphic petrologists.

9. CONCLUSIONS

Iron speciation is a widely used proxy for understanding paleoredox conditions of ancient oceans and lakes; however, it is empirically calibrated on modern sediments and errors could occur through improper limits for interpreted redox conditions, issues with the sequential extraction technique, or diagenetic and metamorphic transformations. Utilizing data from the metamorphic petrology literature of Paleozoic-age sedimentary strata deposited under generally oxic marine conditions, we assessed how variations in metamorphic grade, lithology, and iron speciation pool placement (through different extraction techniques) can quantitatively affect the iron speciation proxy.

Pyrrhotite and iron in carbonates stood out as important minerals that change proxy ratios for our data set. Grouping pyrrhotite in the Fe_{carb} pool (as in older studies or those that do not screen for pyrrhotite) provided significantly lower estimates of Fe_{py}/Fe_{HR} than when it was grouped with the sulfides in Fe_{py}. The correct pool will vary based on the locality, lithology, and metamorphic reactions forming pyrrhotite. Although work on low-grade pelites suggested the pyrrhotite in the studied samples formed from pyrite and should be grouped in the Fe_{py} pool (Ferry 1981), pyrrhotite did form in carbonate lithotypes during progressive metamorphism with minimal decrease in pyrite suggesting iron movement from other pools. Iron carbonates were prevalent across all three types of lithologies and significantly increased the Fe_{HR}/Fe_T ratios suggesting ferruginous depositional conditions. In fact, these carbonates probably formed in anoxic pore fluids associated with early or late diagenetic processes, and do not reflect water column chemistry. With increasing metamorphic grade, the iron within this carbonate transferred to the silicate pool ($Fe_{PRS} + Fe_U$) and significantly decreased the $Fe_{HR}/Fe_{T,}$ which could make the values appear more oxic. Proportionately less carbonate was seen within the pelitic samples and even through increasing metamorphic grade, this lithology preserved the oxic paleoredox information better than psammites and carbonate samples.

Translating iron mineralogy and chemistry from metasedimentary rocks into iron speciation pools and ratios also provided a new perspective to analyze the mobility of iron during progressive metamorphism. Iron moved from iron carbonates to form poorly reactive sheet silicates and unreactive silicate minerals in the biotite, garnet, and amphibole zones. Biotite formation within carbonates occurred in the pelitic schist garnet zone, and by delaying this metamorphic reaction, the formation of unreactive silicates started mainly in the amphibole zone. In carbonates, ilmenite formed at the same time as these unreactive silicates whereas in pelites, ilmenite acted as a reactive oxide phase that was slowly consumed. In pelites, pyrrhotite was also destroyed with increasing grade through progressive desulfurization reactions, but in carbonates, a slight increase in abundance occurred, suggesting the iron for its formation could come from the iron carbonate pool. Many of these reactions have been previously hypothesized by study of metamorphic mineral assemblages, and our work provides some measure of their impact while highlighting the mobile nature of iron in diagenesis and metamorphism.

The petrographic, modal mineralogy, and mineral chemistry approach used here could easily be extended for analysis in sub-greenschist facies rocks to understand the petrogenesis and subsequent mobility of iron during diagenesis. Pairing this technique with isotopic analyses and modeling can also aid in understanding if the system was closed or open and scale of fluid migration. In turn this information can help test the interpretations made from iron speciation data and other paleoredox proxies.

ACKNOWLEDGEMENTS

We thank associate editor Jan Wiederhold, Clark Johnson, Peter Kraal, and one anonymous reviewer for their comments that greatly improved the manuscript. Joseph Kirschvink, Alex Sessions, and John Grotzinger also provided helpful suggestions on an early version of this manuscript. Support for this work was provided by the Agouron Institute (W.W.F.), NSF Graduate Research Fellowship program (S.P.S.) and NASA Earth and Space Fellowship (S.P.S.).

APPENDIX A. SUPPLEMENTARY MATERIALS

Supplementary data associated with this article can be found, in the online version, at https://doi.org/10.1016/j.gca.2017.12.003.

REFERENCES

Algoe C., Stoops G., Vandenberghe R. and Van Ranst E. (2012) Selective dissolution of Fe–Ti oxides—Extractable iron as a criterion for andic properties revisited. *Catena* **92**, 49–54.

Anderson T. F. and Raiswell R. (2004) Sources and mechanisms for the enrichment of highly reactive iron in euxinic Black Sea sediments. *Am. J. Sci.* **304**, 203–233.

Arnold G. L., Anbar A., Barling J. and Lyons T. (2004) Molybdenum isotope evidence for widespread anoxia in mid-Proterozoic oceans. *Science* **304**, 87–90.

Asael D., Tissot F. L., Reinhard C. T., Rouxel O., Dauphas N., Lyons T. W., Ponzevera E., Liorzou C. and Chéron S. (2013) Coupled molybdenum, iron and uranium stable isotopes as oceanic paleoredox proxies during the Paleoproterozoic Shunga Event. *Chem. Geol.* **362**, 193–210.

Bacon J. R. and Davidson C. M. (2008) Is there a future for sequential chemical extraction? *Analyst* **133**, 25–46.

Barnaby R. J. and Rimstidt J. D. (1989) Redox conditions of calcite cementation interpreted from Mn and Fe contents of authigenic calcites. *Geol. Soc. Am. Bull.* **101**, 795–804.

Berner R. A. (1970) Sedimentary pyrite formation. *Am. J. Sci.* **268**, 1–23.

Berner R. A. (1984) Sedimentary pyrite formation: an update. *Geochim. Cosmochim. Acta* **48**, 605–615.

Bickle M., Chapman H., Ferry J., Rumble D. and Fallick A. (1997) Fluid flow and diffusion in the Waterville Limestone,

South—Central Maine: constraints from strontium, oxygen and carbon isotope profiles. *J. Petrol.* **38**, 1489–1512.

Boucot, A. J. (1973). Early Paleozoic brachiopods of the Moose River Synclinorium, Maine, US Professional Paper 784.

Bucher K. and Frey M. (2002) *Petrogenesis of Metamorphic Rocks*. Springer, Berlin.

Burton E. D., Bush R. T. and Sullivan L. A. (2006) Sedimentary iron geochemistry in acidic waterways associated with coastal lowland acid sulfate soils. *Geochim. Cosmochim. Acta* **70**, 5455–5468.

Cabral A., Creaser R., Nägler T., Lehmann B., Voegelin A., Belyatsky B., Pašava J., Gomes A. S., Galbiatti H. and Böttcher M. (2013) Trace-element and multi-isotope geochemistry of Late-Archean black shales in the Carajás iron-ore district, Brazil. *Chem. Geol.* **362**, 91–104.

Canfield D. (1998) A new model for Proterozoic ocean chemistry. *Nature* **396**, 450–453.

Canfield D. E. and Berner R. A. (1987) Dissolution and pyritization of magnetite in anoxie marine sediments. *Geochim. Cosmochim. Acta* **51**, 645–659.

Canfield D. E., Raiswell R., Westrich J. T., Reaves C. M. and Berner R. A. (1986) The use of chromium reduction in the analysis of reduced inorganic sulfur in sediments and shales. *Chem. Geol.* **54**, 149–155.

Canfield D. E., Poulton S. W. and Narbonne G. M. (2007) Late-Neoproterozoic deep-ocean oxygenation and the rise of animal life. *Science* **315**, 92–95.

Canfield D. E., Poulton S. W., Knoll A. H., Narbonne G. M., Ross G., Goldberg T. and Strauss H. (2008) Ferruginous conditions dominated later Neoproterozoic deep-water chemistry. *Science* **321**, 949–952.

Chang S.-B. R. and Kirschvink J. L. (1985) *Possible Biogenic Magnetite Fossils from the Late Miocene Potamida Clays of Crete, Magnetite Biomineralization and Magnetoreception in Organisms*. Springer, pp. 647–669.

Clarkson M., Poulton S., Guilbaud R. and Wood R. (2014) Assessing the utility of Fe/Al and Fe-speciation to record water column redox conditions in carbonate-rich sediments. *Chem. Geol.* **382**, 111–122.

Clarkson M., Wood R., Poulton S., Richoz S., Newton R., Kasemann S., Bowyer F. and Krystyn L. (2016) Dynamic anoxic ferruginous conditions during the end-Permian mass extinction and recovery. *Nat. Commun.* **7**.

Cloud P. E. (1968) Atmospheric and hydrospheric evolution on the primitive earth. *Science* **160**, 729–736.

Connolly J. and Cesare B. (1993) C-O-H-S fluid composition and oxygen fugacity in graphitic metapelites. *J. Metamorph. Geol.* **11**, 379–388.

Copper, P. (2002). Silurian and Devonian reefs: 80 million years of global greenhouse between two ice ages.

Cornwell J. C. and Morse J. W. (1987) The characterization of iron sulfide minerals in anoxic marine sediments. *Mar. Chem.* **22**, 193–206.

Curtis C. (1978) Possible links between sandstone diagenesis and depth-related geochemical reactions occurring in enclosing mudstones. *J. Geol. Soc.* **135**, 107–117.

Denkler K. and Harris A. (1988) Conodont-based determination of the Silurian-Devonian boundary in the Valley and Ridge Province, northern and central Appalachians. *U.S. Geol. Surv. Bull.* **1837**, B1–B13.

Dickson A. J., Rees-Owen R. L., März C., Coe A. L., Cohen A. S., Pancost R. D., Taylor K. and Shcherbinina E. (2014) The spread of marine anoxia on the northern Tethys margin during the Paleocene-Eocene Thermal Maximum. *Paleoceanography* **29**, 471–488.

Dold B. (2003) Speciation of the most soluble phases in a sequential extraction procedure adapted for geochemical studies of copper sulfide mine waste. *J. Geochem. Explor.* **80**, 55–68.

Doll C. G., Cady W. M., Thompson, Jr., J. B. and Billings M. P. (1961) Centennial geologic map of Vermont: Vermont Geol. *Survey, scale* **1**.

Egger M., Rasigraf O., Sapart C. l. J., Jilbert T., Jetten M. S., Röckmann T., van der Veen C., Bânda˘ N., Kartal B. and Ettwig K. F. (2014) Iron-mediated anaerobic oxidation of methane in brackish coastal sediments. *Environ. Sci. Technol.* **49**, 277–283.

El Albani A., Bengtson S., Canfield D. E., Bekker A., Macchiarelli R., Mazurier A., Hammarlund E. U., Boulvais P., Dupuy J.-J. and Fontaine C. (2010) Large colonial organisms with coordinated growth in oxygenated environments 2.1 [thinsp] Gyr ago. *Nature* **466**, 100–104.

Farrell Ú. C., Briggs D. E., Hammarlund E. U., Sperling E. A. and Gaines R. R. (2013) Paleoredox and pyritization of soft-bodied fossils in the Ordovician Frankfort Shale of New York. *Am. J. Sci.* **313**, 452–489.

Ferry J. (1976a) P, T, fCO2 and fH2O during metamorphism of calcareous sediments in the Waterville-Vassalboro area, south-central Maine. *Contrib. Miner. Petrol.* **57**, 119–143.

Ferry J. M. (1976b) Metamorphism of calcareous sediments in the Waterville-Vassalboro area, South-central Maine; mineral reactions and graphical analysis. *Am. J. Sci.* **276**, 841–882.

Ferry J. M. (1979) A map of chemical potential differences within an outcrop. *Am. Mineral.* **64**, 966–985.

Ferry J. M. (1980) A comparative study of geothermometers arld geobarometers in pelitic schists from south-central Maine. *Am. Mineral.* **65**, 720–732.

Ferry J. M. (1981) Petrology of graphitic sulfide-rich schists from south-central Maine: an example of desulfidation during prograde regional metamorphism. *Am. Mineral.* **66**, 908–930.

Ferry J. M. (1983a) Mineral reactions and element migration during metamorphism of calcareous sediments from the Vassalboro Formation, south-central Maine. *Am. Mineral.* **68**, 334–354.

Ferry J. M. (1983b) Regional metamorphism of the Vassalboro Formation, south-central Maine, USA: a case study of the role of fluid in metamorphic petrogenesis. *J. Geol. Soc.* **140**, 551–576.

Ferry J. M. (1984) A biotite isograd in south-central Maine, USA: mineral reactions, fluid transfer, and heat transfer. *J. Petrol.* **25**, 871–893.

Ferry J. M. (1988a) Contrasting mechanisms of fluid flow through adjacent stratigraphic units during regional metamorphism, south-central Maine, USA. *Contrib. Miner. Petrol.* **98**, 1–12.

Ferry J. M. (1988b) Infiltration-driven metamorphism in northern New England, USA. *J. Petrol.* **29**, 1121–1159.

Ferry J. M. (1992) Regional metamorphism of the Waits River Formation, eastern Vermont: delineation of a new type of giant metamorphic hydrothermal system. *J. Petrol.* **33**, 45–94.

Ferry J. M. (1994) Overview of the petrologic record of fluid flow during regional metamorphism in northern New England. *Am. J. Sci.* **294**, 905–988.

Ferry J. M. (2007) The role of volatile transport by diffusion and dispersion in driving biotite-forming reactions during regional metamorphism of the Gile Mountain Formation, Vermont. *Am. Mineral.* **92**, 1288–1302.

Fisher G. W. and Karabinos P. (1980) Stratigraphic sequence of the Gile Mountain and Waits River Formations near Royalton, Vermont. *Geol. Soc. Am. Bull.* **91**, 282–286.

French B. M. (1973) Mineral assemblages in diagenetic and low-grade metamorphic iron-formation. *Econ. Geol.* **68**, 1063–1074.

Geboy N. J., Kaufman A. J., Walker R. J., Misi A., de Oliviera T. F., Miller K. E., Azmy K., Kendall B. and Poulton S. W. (2013) Re–Os age constraints and new observations of Proterozoic glacial deposits in the Vazante Group, Brazil. *Precambr. Res.* **238**, 199–213.

Gilleaudeau G. J. and Kah L. C. (2015) Heterogeneous redox conditions and a shallow chemocline in the Mesoproterozoic ocean: evidence from carbon–sulfur–iron relationships. *Precambr. Res.* **257**, 94–108.

Gillett S. L. (2003) Paleomagnetism of the Notch Peak contact metamorphic aureole, revisited: pyrrhotite from magnetite+ pyrite under submetamorphic conditions. *J. Geophys. Res.-Sol. Ea* **108**.

Haase C. S. (1982) Metamorphic petrology of the Negaunee Iron Formation, Marquette District, northern Michigan; mineralogy, metamorphic reactions, and phase equilibria. *Econ. Geol.* **77**, 60–81.

Hall A. J. (1986) Pyrite-pyrrhotine redox reactions in nature. *Mineral. Mag.* **50**, 223–229.

Hanahan C. (2004) Dissolution of hydroxide minerals in the 1 M sodium acetate, pH 5, extracting solution in sequential extraction schemes. *Environ. Geol.* **45**, 864–868.

Hatch, Jr., N. L. (1988) Some revisions to the stratigraphy and structure of the Connecticut Valley trough, eastern Vermont. *Am. J. Sci.* **288**, 1041–1059.

Hazen R. M., Papineau D., Bleeker W., Downs R. T., Ferry J. M., McCoy T. J., Sverjensky D. A. and Yang H. (2008) Mineral evolution. *Am. Mineral.* **93**, 1693–1720.

Holland H. D. (1984) *The Chemical Evolution of the Atmosphere and Oceans*. Princeton University Press.

Holland T. and Powell R. (1998) An internally consistent thermodynamic data set for phases of petrological interest. *J. Metamorph. Geol.* **16**, 309–343.

Hsieh Y.-P., Chung S.-W., Tsau Y.-J. and Sue C.-T. (2002) Analysis of sulfides in the presence of ferric minerals by diffusion methods. *Chem. Geol.* **182**, 195–201.

Hueber F. M., Bothner W. A., Hatch N. L., Finney S. C. and Aleinikoff J. N. (1990) Devonian plants from southern Quebec and northern New Hampshire and the age of the Connecticut Valley trough. *Am. J. Sci.* **290**, 360–395.

Hughson, R. C. and Stearn, C. W. (1988). Upper Silurian Reefal Facies of the Memphremagog-Marbleton Area, Eastern Townships, Quebec Appalachians.

Izon G., Zerkle A. L., Williford K. H., Farquhar J., Poulton S. W. and Claire M. W. (2017) Biological regulation of atmospheric chemistry en route to planetary oxygenation. *Proc. Natl. Acad. Sci.* **114**, E2571–E2579.

Jin C., Li C., Algeo T. J., Planavsky N. J., Cui H., Yang X., Zhao Y., Zhang X. and Xie S. (2016) A highly redox-heterogeneous ocean in South China during the early Cambrian (~529–514 Ma): Implications for biota-environment co-evolution. *Earth Planet. Sci. Lett.* **441**, 38–51.

Johnston D. T., Poulton S. W., Dehler C., Porter S., Husson J., Canfield D. E. and Knoll A. H. (2010) An emerging picture of Neoproterozoic ocean chemistry: Insights from the Chuar Group, Grand Canyon, USA. *Earth Planet. Sci. Lett.* **290**, 64–73.

Johnston D., Poulton S., Goldberg T., Sergeev V., Podkovyrov V., Vorob'eva N., Bekker A. and Knoll A. (2012) Late Ediacaran redox stability and metazoan evolution. *Earth Planet. Sci. Lett.* **335**, 25–35.

Johnston D., Poulton S., Tosca N., O'brien T., Halverson G., Schrag D. and Macdonald F. (2013) Searching for an oxygenation event in the fossiliferous Ediacaran of northwestern Canada. *Chem. Geol.* **362**, 273–286.

Jones J. (1972) An almandine garnet isograd in the Rogers Pass area, British Columbia: the nature of the reaction and an estimation of the physical conditions during its formation. *Contrib. Miner. Petrol.* **37**, 291–306.

Kendall B., Creaser R. A., Gordon G. W. and Anbar A. D. (2009) Re–Os and Mo isotope systematics of black shales from the Middle Proterozoic Velkerri and Wollogorang formations, McArthur Basin, northern Australia. *Geochim. Cosmochim. Acta* **73**, 2534–2558.

Kissin S. and Scott S. (1982) Phase relations involving pyrrhotite below 350 degrees C. *Econ. Geol.* **77**, 1739–1754.

Klein C. (1966) Mineralogy and petrology of the metamorphosed Wabush Iron Formation, southwestern Labrador. *J. Petrol.* **7**, 246–305.

La Force M. J. and Fendorf S. (2000) Solid-phase iron characterization during common selective sequential extractions. *Soil Sci. Soc. Am. J.* **64**, 1608–1615.

Léger A. and Ferry J. M. (1991) Highly aluminous hornblende from low-pressure metacarbonates and a preliminary thermodynamic model for the Al content of calcific amphibole. *Am. Mineral.* **76**, 1002–1017.

Léger A. and Ferry J. (1993) Fluid infiltration and regional metamorphism of the Waits River Formation, North-east Vermont, USA. *J. Metamorph. Geol.* **11**, 3–29.

Leventhal J. and Taylor C. (1990) Comparison of methods to determine degree of pyritization. *Geochim. Cosmochim. Acta* **54**, 2621–2625.

Li C., Planavsky N. J., Love G. D., Reinhard C. T., Hardisty D., Feng L., Bates S. M., Huang J., Zhang Q. and Chu X. (2015) Marine redox conditions in the middle Proterozoic ocean and isotopic constraints on authigenic carbonate formation: Insights from the Chuanlinggou Formation, Yanshan Basin, North China. *Geochim. Cosmochim. Acta* **150**, 90–105.

Li Y. and Schoonmaker J. (2003) Chemical composition and mineralogy of marine sediments. In *Sediments, Diagenesis, and Sedimentary Rocks: Treatise on Geochemistry* (ed. F. T. Mackenzie).

Lodders K. and Fegley B. (1997) An oxygen isotope model for the composition of Mars. *Icarus* **126**, 373–394.

Ludman, A. (2014). SHRIMP U-Pb geochronology of pre-Acadian Silurian basins of central and east-central Maine and the Pocomoonshire pluton: Diverse sources, rapid sedimentation, tectonism, and intrusion.

Lyons J. B. (1955) Geology of the Hanover quadrangle, New Hampshire-Vermont. *Geol. Soc. Am. Bull.* **66**, 105–146.

März C., Poulton S., Beckmann B., Küster K., Wagner T. and Kasten S. (2008) Redox sensitivity of P cycling during marine black shale formation: dynamics of sulfidic and anoxic, non-sulfidic bottom waters. *Geochim. Cosmochim. Acta* **72**, 3703–3717.

McWilliams C. K., Walsh G. J. and Wintsch R. P. (2010) Silurian-Devonian age and tectonic setting of the Connecticut Valley-Gaspe trough in Vermont based on U-Pb SHRIMP analyses of detrital zircons. *Am. J. Sci.* **310**, 325–363.

McWilliams C. K., Kunk M. J., Wintsch R. P. and Bish D. L. (2013) Determining ages of multiple muscovite-bearing foliations in phyllonites using the 40Ar/39Ar step heating method: Applications to the Alleghanian orogeny in central New England. *Am. J. Sci.* **313**, 996–1016.

Melezhik V. A., Fallick A. E., Brasier A. T. and Lepland A. (2015) Carbonate deposition in the Palaeoproterozoic Onega basin from Fennoscandia: a spotlight on the transition from the Lomagundi-Jatuli to Shunga events. *Earth-Sci. Rev.* **147**, 65–98.

Moench, R. H., Boone, G., Bothner, W., Boudette, E., Hatch, Jr., N., Hussey, III, A., Marvinney, R. (1995). Geologic Map of the Sherbrooke-Lewiston Area, Maine, New Hampshire, and

Vermont, United States, and Quebec, Canada. US Geological Survey.

Nesbitt B. and Kelly W. (1980) Metamorphic zonation of sulfides, oxides, and graphite in and around the orebodies at Ducktown, Tennessee. *Econ. Geol.* **75**, 1010–1021.

Och L. M., Shields-Zhou G. A., Poulton S. W., Manning C., Thirlwall M. F., Li D., Chen X., Ling H., Osborn T. and Cremonese L. (2013) Redox changes in Early Cambrian black shales at Xiaotan section, Yunnan Province, south China. *Precambr. Res.* **225**, 166–189.

Och L. M., Cremonese L., Shields-Zhou G. A., Poulton S. W., Struck U., Ling H., Li D., Chen X., Manning C. and Thirlwall M. (2016) Palaeoceanographic controls on spatial redox distribution over the Yangtze Platform during the Ediacaran-Cambrian transition. *Sedimentology*.

Osberg P. H. (1968) *Stratigraphy, Structural Geology, and Metamorphism of the Waterville-Vassalboro Area*. Maine Geological Survey, Maine.

Osberg P. (1988) Geologic relations within the shale-wacke sequence in south-central Maine. *Stud. Mar. Geol.* **1**, 51–73.

Osberg P. H., Tull J. F., Robinson P., Hon R. and Butler J. R. (1989) The Acadian orogen. The Appalachian-Ouachita orogen in the United States, The geology of North America. *Geol. Soc. Am., Boulder* **2**, 179–232.

Pankiwskyj K. A., Ludman A., Griffin J. R. and Berry W. (1976) Stratigraphic relationships on the southeast limb of the Merrimack synclinorium in central and west-central Maine. *Geol. Soc. Am. Mem.* **146**, 263–280.

Partin C., Bekker A., Corrigan D., Modeland S., Francis D. and Davis D. (2014) Sedimentological and geochemical basin analysis of the Paleoproterozoic Penrhyn and Piling groups of Arctic Canada. *Precambr. Res.* **251**, 80–101.

Partin C., Bekker A., Planavsky N. and Lyons T. (2015) Euxinic conditions recorded in the ca. 1.93 Ga Bravo Lake Formation, Nunavut (Canada): Implications for oceanic redox evolution. *Chem. Geol.* **417**, 148–162.

Penniston-Dorland S. C. and Ferry J. M. (2006) Development of spatial variations in reaction progress during regional metamorphism of micaceous carbonate rocks, northern New England. *Am. J. Sci.* **306**, 475–524.

Penniston-Dorland S. C. and Ferry J. M. (2008) Element mobility and scale of mass transport in the formation of quartz veins during regional metamorphism of the Waits River Formation, east-central Vermont. *Am. Mineral.* **93**, 7–21.

Planavsky N. J., McGoldrick P., Scott C. T., Li C., Reinhard C. T., Kelly A. E., Chu X., Bekker A., Love G. D. and Lyons T. W. (2011) Widespread iron-rich conditions in the mid-Proterozoic ocean. *Nature* **477**, 448–451.

Poulton S. and Raiswell R. (2002) The low-temperature geochemical cycle of iron: from continental fluxes to marine sediment deposition. *Am. J. Sci.* **302**, 774–805.

Poulton S. W. and Canfield D. E. (2005) Development of a sequential extraction procedure for iron: implications for iron partitioning in continentally derived particulates. *Chem. Geol.* **214**, 209–221.

Poulton S. W. and Canfield D. E. (2011) Ferruginous conditions: a dominant feature of the ocean through Earth's history. *Elements* **7**, 107–112.

Poulton S. W., Fralick P. W. and Canfield D. E. (2010) Spatial variability in oceanic redox structure 1.8 billion years ago. *Nat. Geosci.* **3**, 486–490.

Praharaj T. and Fortin D. (2004) Determination of acid volatile sulfides and chromium reducible sulfides in Cu-Zn and Au mine tailings. *Water Air Soil Pollut.* **155**, 35–50.

Raiswell R. and Berner R. A. (1985) Pyrite formation in euxinic and semi-euxinic sediments. *Am. J. Sci.* **285**, 710–724.

Raiswell R., Buckley F., Berner R. A. and Anderson T. (1988) Degree of pyritization of iron as a paleoenvironmental indicator of bottom-water oxygenation. *J. Sediment. Res.* **58**.

Raiswell R., Canfield D. and Berner R. (1994) A comparison of iron extraction methods for the determination of degree of pyritisation and the recognition of iron-limited pyrite formation. *Chem. Geol.* **111**, 101–110.

Raiswell R. and Canfield D. E. (1998) Sources of iron for pyrite formation in marine sediments. *Am. J. Sci.* **298**, 219–245.

Raiswell R. and Canfield D. E. (2012) The iron biogeochemical cycle past and present. *Geochem. Perspect.* **1**, 1–2.

Raiswell R., Newton R. and Wignall P. (2001) An indicator of water-column anoxia: resolution of biofacies variations in the Kimmeridge Clay (Upper Jurassic, UK). *J. Sediment. Res.* **71**, 286–294.

Raiswell R., Reinhard C. T., Derkowski A., Owens J., Bottrell S. H., Anbar A. D. and Lyons T. W. (2011) Formation of syngenetic and early diagenetic iron minerals in the late Archean Mt. McRae Shale, Hamersley Basin, Australia: New insights on the patterns, controls and paleoenvironmental implications of authigenic mineral formation. *Geochim. Cosmochim. Acta* **75**, 1072–1087.

Rankin D. and Tucker R. (2009) *Bronson Hill and Connecticut Valley sequences in the Stone Mountain area, Northeast Kingdom, Vermont, Guidebook for Field Trips in the Northeast Kingdom of Vermont and Adjacent Regions: New England Intercollegiate Geological Conference, 101st Annual Meeting: Lyndonville*. Lyndon State College, Vermont, pp. 187–198.

Reinhard C. T., Raiswell R., Scott C., Anbar A. D. and Lyons T. W. (2009) A late Archean sulfidic sea stimulated by early oxidative weathering of the continents. *Science* **326**, 713–716.

Reinhard C. T., Lyons T. W., Rouxel O., Asael D., Dauphas N. and Kump L. R. (2013) 7.10.4 Iron Speciaiton and Isotope Perspectives on Palaeoproterozoic Water Column Chemistry. In *Reading the Archive of Earth's Oxygenation* (eds. V. Melezhik, A. R. Prave, E. J. Hanski, A. E. Fallick, A. Lepland, L. R. Kump and H. Strauss). Springer, Berlin Heidelberg, pp. 1483–1492.

Reuschel M., Melezhik V. and Strauss H. (2012) Sulfur isotopic trends and iron speciation from the c. 2.0 Ga Pilgujärvi Sedimentary Formation. NW Russia. *Precambr. Res.* **196**, 193–203.

Robie R. A., Bethke P. M. and Beardsley K. M. (1967) *Selected X-ray Crystallographic Data, Molar Volumes, and Densities of Minerals and Related Substances*. US Government Printing Office.

Roscoe, S. (1969). Huronian rocks and uraniferous conglomerates in the Canadian Shield. Geological Survey of Canada, p. 193.

Rye R. and Holland H. D. (1998) Paleosols and the evolution of atmospheric oxygen: a critical review. *Am. J. Sci.* **298**, 621–672.

Scholle P. A. and Ulmer-Scholle D. S. (2003) *A Color Guide to the Petrography of Carbonate Rocks: Grains, Textures, Porosity, Diagenesis*. AAPG.

Schumann R., Stewart W., Miller S., Kawashima N., Li J. and Smart R. (2012) Acid–base accounting assessment of mine wastes using the chromium reducible sulfur method. *Sci. Total Environ.* **424**, 289–296.

Shen Y., Canfield D. E. and Knoll A. H. (2002) Middle Proterozoic ocean chemistry: evidence from the McArthur Basin, northern Australia. *Am. J. Sci.* **302**, 81–109.

Spear F. S. and Harrison T. M. (1989) Geochronologic studies in central New England I: Evidence for pre-Acadian metamorphism in eastern Vermont. *Geology* **17**, 181–184.

Sperling E. A., Halverson G. P., Knoll A. H., Macdonald F. A. and Johnston D. T. (2013) A basin redox transect at the dawn of animal life. *Earth Planet. Sci. Lett.* **371**, 143–155.

Sperling E., Rooney A., Hays L., Sergeev V., Vorob'eva N., Sergeeva N., Selby D., Johnston D. and Knoll A. (2014) Redox heterogeneity of subsurface waters in the Mesoproterozoic ocean. *Geobiology* **12**, 373–386.

Sperling E. A., Wolock C. J., Morgan A. S., Gill B. C., Kunzmann M., Halverson G. P., Macdonald F. A., Knoll A. H. and Johnston D. T. (2015) Statistical analysis of iron geochemical data suggests limited late Proterozoic oxygenation. *Nature* **523**, 451–454.

Thompson, Jr., J. B. and Norton S. A. (1968) Paleozoic regional metamorphism in New England and adjacent areas. In *Studies of Appalachian Geology: Northern and Maritime* (eds. E. Zen, W. S. White, J. B. Hadley and , Jr. J. B. Thompson). Wiley, New York, pp. 319–327.

Thompson, Jr., J. B., Robinson P., Clifford T. N. and Trask, Jr., N. J. (1968) Nappes and gneiss domes in west-central New England. In *Studies of Appalachian Geology: Northern and Maritime* (eds. E. Zen, W. S. White, J. B. Hadley and , Jr. J. B. Thompson). Wiley, New York, pp. 203–218.

Tomkins A. G. (2010) Windows of metamorphic sulfur liberation in the crust: implications for gold deposit genesis. *Geochim. Cosmochim. Acta* **74**, 3246–3259.

Toulmin P. and Barton P. B. (1964) A thermodynamic study of pyrite and pyrrhotite. *Geochim. Cosmochim. Acta* **28**, 641–671.

Tracy R. J. and Robinson P. (1988) Silicate-sulfide-oxide-fluid reactions in granulite-grade pelitic rocks, central Massachusetts. *Am. J. Sci.* **288**, 45–74.

Tucker R., Osberg P. and Berry H. (2001) The geology of a part of Acadia and the nature of the Acadian orogeny across central and eastern Maine. *Am. J. Sci.* **301**, 205–260.

Vaughan D. J. and Lennie A. R. (1991) The iron sulphide minerals: their chemistry and role in nature. *Sci. Prog.*(1933-), 371–388.

Vaughan D. and Craig J. (1997) Sulfide ore mineral stabilities, morphologies, and intergrowth textures. *Geochem. Hydrothermal ore deposits* **3**, 367–434.

Volkov I. (1961) Iron sulphide, their interrelations and transformations in the sediments of the Black Sea. *Akademiya Nauk SSSR Instituta Okeanologii Trudy* **50**, 68–92.

Walker R. and James N. (1992) *Facies models: Response to sea level change*. Geological Association of Canada, St. John's, Newfoundland.

Warren J. (2000) Dolomite: occurrence, evolution and economically important associations. *Earth-Sci. Rev.* **52**, 1–81.

Warshauer S. M. and Smosna R. (1977) Paleoecologic controls of the ostracode communities in the Tonoloway Limestone (Silurian; Pridoli) of the central Appalachians. *Aspects Ecol. Zoogeogr. Recent Fossil Ostracoda*, 475–485.

Watkins R. (1996) Skeletal composition of Silurian benthic marine faunas. *Palaios*, 550–558.

Whitney D. L. and Evans B. W. (2010) Abbreviations for names of rock-forming minerals. *Am. Mineral.* **95**, 185.

Wilkin R. and Barnes H. (1997) Formation processes of framboidal pyrite. *Geochim. Cosmochim. Acta* **61**, 323–339.

Wilkin R., Barnes H. and Brantley S. (1996) The size distribution of framboidal pyrite in modern sediments: an indicator of redox conditions. *Geochim. Cosmochim. Acta* **60**, 3897–3912.

Wing B. A., Ferry J. M. and Harrison T. M. (2003) Prograde destruction and formation of monazite and allanite during contact and regional metamorphism of pelites: petrology and geochronology. *Contrib. Miner. Petrol.* **145**, 228–250.

Wood R., Poulton S., Prave A., Hoffmann K.-H., Clarkson M., Guilbaud R., Lyne J., Tostevin R., Bowyer F. and Penny A. (2015) Dynamic redox conditions control late Ediacaran metazoan ecosystems in the Nama Group, Namibia. *Precambr. Res.* **261**, 252–271.

Woodland B. G. (1977) Structural analysis of the Silurian-Devonian rocks of the Royalton area, Vermont. *Geol. Soc. Am. Bull.* **88**, 1111–1123.

Zhou T., Phillips G. N., Dong G. and Myers R. E. (1995) Pyrrhotite in the Witwatersrand gold fields, South Africa. *Econ. Geol.* **90**, 2361–2369.

Associate editor: Jan G. Wiederhold